

${}^5_{\Lambda\Lambda}\text{H}$ and ${}^5_{\Lambda\Lambda}\text{He}$ Hypernuclei revisited in Halo/Cluster Effective Theory

Ghanashyam Meher^{1,*} and Udit Raha^{1,†}

¹*Department of Physics, Indian Institute of Technology Guwahati, 781 039 Assam, India*

The $J = 1/2$ iso-doublet double- Λ hypernuclei, namely, ${}^5_{\Lambda\Lambda}\text{H}$ and ${}^5_{\Lambda\Lambda}\text{He}$, are examined as the three-body cluster states, $\Lambda\Lambda t$ ($t \equiv {}^3\text{H}$ or triton) and $\Lambda\Lambda h$ ($h \equiv {}^3\text{He}$ or helion), respectively, in a model independent framework utilizing pionless halo effective field theory. Both singlet and triplet states of the ΛT ($T \equiv t, h$) subsystems are used in the elastic channel for the study of ${}^4_{\Lambda}\text{H}-\Lambda$ and ${}^4_{\Lambda}\text{He}-\Lambda$ scattering processes. A prototypical leading order investigation yields a $\Lambda\Lambda$ separation energy ($B_{\Lambda\Lambda}$) of ${}^5_{\Lambda\Lambda}\text{He}$ greater than that of ${}^5_{\Lambda\Lambda}\text{H}$, in agreement with the existing results from rigorous Faddeev calculation analyses using potential model framework. In particular, our study of the sharp momentum cut-off dependence of the non-asymptotic solutions to the coupled integral equations, upon normalization with respect to a single potential model predicted ($B_{\Lambda\Lambda}$, $a_{\Lambda\Lambda}$) data point ($a_{\Lambda\Lambda}$ being the S-wave $\Lambda\Lambda$ scattering length) for each $\Lambda\Lambda T$ iso-doublet, yields results with reasonably good agreement with potential model analyses for cut-off scales close to $\Lambda_c \sim 230 - 240$ MeV. This is consistent with low-energy $\Lambda\Lambda$ interaction mechanism dominated by two π or σ meson exchange. Finally, we present a preliminary estimate of the S-wave $\Lambda\Lambda T$ three-body scattering lengths at the leading order in the effective theory for several input values of $a_{\Lambda\Lambda}$ which were earlier predicted from several existing phenomenological analyses.

I. INTRODUCTION

The recent experimental [1–5] and theoretical [6–15] investigations on the doubly strange ($S = -2$) s -shell light hypernuclei, such as ${}^4_{\Lambda\Lambda}\text{H}$, ${}^4_{\Lambda\Lambda}\text{He}$, ${}^5_{\Lambda\Lambda}\text{H}$, ${}^5_{\Lambda\Lambda}\text{He}$ and ${}^6_{\Lambda\Lambda}\text{He}$ have brought keen interest in the study of exotic hypernuclei in the strangeness nuclear physics community over the last two decades. Such multi-strange systems can provide stringent tests for probing the microscopic mechanism for the flavor SU(3) baryon-baryon interaction in the strangeness $S = -2$ channel. In particular, essential information about $\Lambda - \Lambda$ interaction are expected to be obtained from these studies which may be the key in resolving at least two of the most prominent longstanding puzzles:

- first, on the existence of the controversial deeply bound H -dibaryon, an exotic 6-quark ($J = 0, I = 0$) state, originally predicted in a *bag-model* analysis by R. Jaffe in 1977 [6];
- second, on the baffling issue, so-called the “hyperon puzzle”, regarding the maximum allowed mass of neutron stars posing a challenge to their canonical mass range and casting doubt on the existence of hyperon matter in stellar cores.

Different perspectives regarding the existence of the H -particle have been obtained in *ab initio* calculations since then. For example, Lattice QCD simulations [16, 17] with significantly larger pion masses seemed to yield positive indications of the existence of such a bound state, albeit a shallow one in the SU(3) limit. However, apparently by going to the physical limit, it tends to get

pushed to the threshold and eventually dissolves into the continuum when the SU(3) breaking effects are considered. Again in a *dispersion relations* based analysis on the ${}^{12}\text{C}(K^-, K^+\Lambda\Lambda X)$ reaction [18] a rather small magnitude of the $\Lambda\Lambda$ ${}^1\text{S}_0$ scattering length, namely, $a_{\Lambda\Lambda} = -1.2 \pm 0.6$ fm was predicted, casting a significant doubt on the existence of the H -particle. Furthermore, a range of $-0.55 \text{ fm}^{-1} \leq 1/a_{\Lambda\Lambda} \leq -1.25$ fm was set in a more recent theoretical investigation based on Au+Au *Relativistic Heavy-Ion Collisions* [19]. Although these analyses are somewhat equivocal in their resolution of the H -particle conjecture, their results evidently converge to the consensus of a weakly attractive nature of $\Lambda - \Lambda$ interaction with no deeply bound state. This unfortunately implies a considerable softening of the *equation of state* of hyperonic matter which further aggravates the hyperon anomaly.

With the recent discovery of ${}^6_{\Lambda\Lambda}\text{He}$ in the hybrid-emulsion experiment KEK-E373 [1], so-called the “NAGARA” event, along with indications of the conjectured ${}^4_{\Lambda\Lambda}\text{H}$ bound state in the BNL-AGS E906 production experiment [2], arguments on the existence of double- Λ hypernuclei have gained a firm foothold fostering a prolific area of modern theoretical nuclear research. A whole gamut of theoretical investigations on the double- Λ hypernuclei followed since then. However, these investigations so far have been focusing towards establishing phenomenological potential models, such as that of the $J = 1/2$ iso-doublet system (mirror nuclei), namely, the ${}^5_{\Lambda\Lambda}\text{H}$ and ${}^5_{\Lambda\Lambda}\text{He}$ [8–13]. All these analyses either involve rigorous three-body Faddeev calculations or variational Monte Carlo simulations based on $\Lambda\Lambda{}^3\text{H}$ and $\Lambda\Lambda{}^3\text{He}$ three-body cluster models, when little is currently known regarding the bound state features of these systems from experimental observations. In some of these theoretical analyses the binding energy difference between the two isospin partners has been studied using dynamical effects of mixing between different channels, such

* ghanashyam@iitg.ac.in

† udit.raha@iitg.ernet.in

as ΣN , $\Sigma\Sigma$ and ΞN . Of these, it is believed that the dominant contribution arises from the $\Lambda\Lambda - \Xi N$ mixing channel. Because of this channel coupling the value of the three-body hypernuclear binding energy (otherwise, commonly regarded in literature as the double- Λ separation energy) $B_{\Lambda\Lambda}$ in ${}^5_{\Lambda\Lambda}\text{He}$ significantly exceeds that of ${}^5_{\Lambda\Lambda}\text{H}$. Since these results are intrinsically model-dependent with conclusions often conflicting between different model approaches, it is timely to supplement the multitude of the existing model results with a general model-independent predictions based on universal arguments in few-body systems. To this end, in this work we re-examine the plausible nature of the double- Λ mirror hypernuclei (${}^5_{\Lambda\Lambda}\text{H}$, ${}^5_{\Lambda\Lambda}\text{He}$), and investigate the correlations between their bound state characteristics and the S-wave ${}^4_{\Lambda}\text{H} - \Lambda$ and ${}^4_{\Lambda}\text{He} - \Lambda$ scattering processes, respectively, below the ${}^4_{\Lambda}\text{H}$ and ${}^4_{\Lambda}\text{He}$ breakup thresholds. In this way, through a prototypical model-independent qualitative study we hope to shed light on the character of the low-energy $\Lambda - \Lambda$ interactions expected in finite systems and bulk of nuclear matter.

A low-energy effective field theory (EFT) constitutes a systematic model-independent approach with low-energy observables expanded in a perturbative expansion in terms of a small expansion parameter, namely, $\epsilon \sim Q/\Lambda_H \ll 1$, where Q is the typical momentum scale and Λ_H is the ultraviolet (UV) cut-off scale which limits the applicability of the perturbative scheme. The effective degrees of freedom consistent with the low-energy symmetries of the system are then identified in terms of which the Lagrangian of the system is constructed and expanded in increasing order of derivatives interactions with the corresponding coefficients (low-energy constants) fixed from phenomenological data. The heavy degrees of freedom above the hard scale Λ_H are integrated out and their effects are implicitly encoded in these couplings. In the so-called *halo/cluster* EFT formalism, the ${}^5_{\Lambda\Lambda}\text{H}$ and ${}^5_{\Lambda\Lambda}\text{He}$ systems can be regarded as the double- Λ *halo*-nuclear states, namely, $\Lambda\Lambda t$ ($t \equiv {}^3\text{H}$, i.e., the *triton*) and $\Lambda\Lambda h$ ($h \equiv {}^3\text{He}$, i.e., the *helion*), respectively, with $T \equiv t$, h being the compact core that can be considered elementary at typical momenta Q chosen well below the ${}^4_{\Lambda}\text{H}$ and ${}^4_{\Lambda}\text{He}$ breakup scales.

The recent emulsion works of Refs. [3, 5] have indicated evidences of particle stable states of ${}^4_{\Lambda}\text{H}$ and ${}^4_{\Lambda}\text{He}$ hypernuclei. From the observed γ -ray transitions between the different hyperfine levels, the extracted $J^P = 0^+$ ground state energies ($\mathcal{B}_{\Lambda}[0^+]$) of ${}^4_{\Lambda}\text{H}$ and ${}^4_{\Lambda}\text{He}$ are 2.04 ± 0.04 MeV and 2.39 ± 0.03 MeV, respectively, whereas the $J^P = 1^+$ first excited state energies ($\mathcal{B}_{\Lambda}[1^+]$) are 0.96 ± 0.04 MeV and 1.24 ± 0.05 MeV, respectively. Thus, the typical momentum scale Q associated with the system can be identified with the first excited state binding momentum $Q \sim \sqrt{2\mu_{\Lambda T}\mathcal{B}_{\Lambda}[1^+]} \approx 57$ MeV (62 MeV) for ${}^4_{\Lambda}\text{H}$ (${}^4_{\Lambda}\text{He}$), with $\mu_{\Lambda T}$ being the reduced mass of the ΛT subsystem. On the other hand, the experimental binding energies (\mathcal{B}_T) of the triton and helion cores are 8.48 MeV and 7.72 MeV, respectively, so that *breakdown* scale of

our EFT framework may be associated with the corresponding binding momentum scale $\Lambda_H \sim \sqrt{2\mu_{dN}\mathcal{B}_T} \sim m_{\pi}$ of the core, with μ_{dN} being the reduced mass of the deuteron (d) and nucleon (N) system, and m_{π} , the pion mass. Consequently, the numerical value of our EFT expansion parameter is conservatively estimated to be at the most $\epsilon \sim \gamma_{\Lambda T}/m_{\pi} \sim 0.38$.

A practical computational framework for investigating three-body dynamics is thus provided by the so-called *pi-onless* EFT (i.e., $\not{\pi}$ EFT) without explicit pions which has become a popular tool for investigating shallow bound state systems of nucleons and other hadrons (for reviews and recent works, e.g., see Refs. [7, 20–30] and other references therein.) Such a framework provides the most general approach to handle the dynamics of finely tuned systems with large scattering lengths and cross sections nearly saturating the unitary bound. This happens presumably in the vicinities of non-trivial renormalization group (RG) fixed points of the two-body contact couplings. Recently, a large number of works on $\not{\pi}$ EFT have dealt with the low-energy universal physics aspects of three-body systems. A typical signature of the onset of such universality is the appearance of a RG limit cycle due to the breakdown from an exact to a discrete scaling invariance, and consequently the emergence of a geometric tower of arbitrary shallow three-body Efimov bound states [26, 31]. In the context of hypernuclear physics, the Efimov effect and its role in the prediction and formation of three-body exotic bound states have been discussed in a number of recent theoretical works [7, 27–29, 32] based on $\not{\pi}$ EFT analyses at leading order. In the following we use a similar set-up to investigate whether Efimov effect can be manifest in the $\Lambda\Lambda T$ system. However, the current paucity of phenomenological information to constrain the various low-energy parameters of theory is a major drawback of our approach which impedes a robust prediction of the existence of Efimov-like bound states in the ${}^5_{\Lambda\Lambda}\text{H}$ and ${}^5_{\Lambda\Lambda}\text{He}$ systems. As demonstrated in our analysis, a crucial piece of information required as input to the EFT analysis is a three-body datum, e.g., the binding energy $B_{\Lambda\Lambda}$ or the corresponding scattering length $a_{\Lambda\Lambda T}$, neither of which exists currently. Thus, instead of focusing on the feasibility of realistic bound states for these cluster systems, our primary goal in this work is to present a simplistic but nonetheless general assessment of the RG behavior of the three-body contact interactions whose dynamics may be vital to the underlying mechanism of Efimov-like states. For the purpose of quantitative demonstration, as the phenomenological input to our EFT analysis we rely on some prominent results from pre-existing potential model analyses. In particular, as demonstrated in Sec. III, using a recent potential model prediction for the hypernuclear binding energies $B_{\Lambda\Lambda}$, based on a Faddeev calculation analysis [8], along with phenomenological data for the S-wave double- Λ scattering lengths $a_{\Lambda\Lambda}$ [33, 34], we estimated the corresponding three-body scattering lengths $a_{\Lambda\Lambda T}$.

The paper is organized as follows. In Sec. II we present

the basic theoretical set-up of our $\not\epsilon$ EFT formalism which includes a brief discussion on the most general LO effective Lagrangian needed for our analysis. Furthermore with the appropriate choice of the LO three-body counterterms, we display the coupled system of three-body integral equations and demonstrate how their asymptotic behavior leads to the emergence of RG limit cycles in these systems. Sec. III contains our results that follow from the numerical evaluations of the integral equations. In addition, with an essential input from a prominent potential model analysis that serves to normalize our numerically generated data, we present a preliminary estimate of the $\Lambda\Lambda T$ scattering lengths for the two mirror hypernuclei. Finally, in Sec. IV we summarize our results and present the conclusions. For pedagogical completeness, a brief discussion on the one- and two-body non-relativistic propagators in $\not\epsilon$ EFT are presented in the Appendix.

II. THEORETICAL FRAMEWORK

A. Effective Lagrangian

We use the theoretical framework of pionless effective field theory to investigate the bound states of the double- Λ hypernuclear mirror systems (${}_{\Lambda\Lambda}^5\text{H}$, ${}_{\Lambda\Lambda}^5\text{He}$). In this approach the effective Lagrangian is constructed manifestly non-relativistic on the basis of the available symmetries of the relevant low-energy degrees of freedom. In our case, the explicit elementary degrees of freedom involve two Λ -hyperon *halo* fields and a generic *core* field, $T \equiv t, h$, representing one of the two mirror (isospin) partners, namely, the triton (t) or the helion (h). In addition, it is convenient to introduce auxiliary dimer fields to unitarize and renormalize the two-body sectors [24, 26, 35–37]. Our formalism includes three such dimer fields, namely, the spin-singlet (${}^1\text{S}_0$) field $u_0 \equiv (\Lambda T)_s$, the spin-triplet (${}^3\text{S}_1$) field $u_1 \equiv (\Lambda T)_t$, and the spin-singlet $\Lambda\Lambda$ -dibaryon field $u_s \equiv (\Lambda\Lambda)_s$. It must be noted that the dimer states $u_{0,1}$ already correspond to the experimentally observed spin-singlet (0^+) ground state and spin-triplet (1^+) excited state of the mirror hypernuclei (${}_{\Lambda}^4\text{H}$, ${}_{\Lambda}^4\text{He}$).

The full non-relativistic $\not\epsilon$ EFT Lagrangian can be expressed as the following string of terms:

$$\mathcal{L} = \mathcal{L}_{\Lambda} + \mathcal{L}_T + \mathcal{L}_{u_0} + \mathcal{L}_{u_1} + \mathcal{L}_{u_s} + \mathcal{L}_{3\text{-body}}. \quad (1)$$

The one-body Lagrangian containing the contributions of the elementary fields, namely, the Λ -hyperon field and the spin-1/2 core field T , is given as

$$\mathcal{L}_{\Lambda} = \Lambda^{\dagger} \left[i(v \cdot \partial) + \frac{(v \cdot \partial)^2 - \partial^2}{2M_{\Lambda}} + \dots \right] \Lambda, \quad (2)$$

$$\mathcal{L}_T = T^{\dagger} \left[i(v \cdot \partial) + \frac{(v \cdot \partial)^2 - \partial^2}{2M_T} + \dots \right] T, \quad (3)$$

where M_{Λ} and M_T are the respective masses of the Λ -hyperon and the core T . Next we display the two-body

Lagrangian terms:

$$\begin{aligned} \mathcal{L}_{u_0} = & -u_0^{\dagger} \left[i(v \cdot \partial) + \frac{(v \cdot \partial)^2 - \partial^2}{2(M_{\Lambda} + M_T)} + \dots \right] u_0 \\ & - y_0 \left[u_0^{\dagger} \left(T^T \hat{\mathbb{P}}_{(\Lambda T)}^{(1\text{S}_0)} \Lambda \right) + \text{h.c.} \right] + \dots, \end{aligned} \quad (4)$$

$$\begin{aligned} \mathcal{L}_{u_1} = & -(u_1)_j^{\dagger} \left[i(v \cdot \partial) + \frac{(v \cdot \partial)^2 - \partial^2}{2(M_{\Lambda} + M_T)} + \dots \right] (u_1)_j \\ & - y_1 \left[(u_1)_j^{\dagger} \left(T^T \hat{\mathbb{P}}_{(\Lambda T)_j}^{(3\text{S}_1)} \Lambda \right) + \text{h.c.} \right] + \dots, \end{aligned} \quad (5)$$

$$\begin{aligned} \mathcal{L}_{u_s} = & -u_s^{\dagger} \left[i(v \cdot \partial) + \frac{(v \cdot \partial)^2 - \partial^2}{4M_{\Lambda}} + \dots \right] u_s \\ & - y_s \left[u_s^{\dagger} \left(\Lambda^T \hat{\mathbb{P}}_{(\Lambda\Lambda)}^{(1\text{S}_0)} \Lambda \right) + \text{h.c.} \right] + \dots, \end{aligned} \quad (6)$$

where the spin-singlet and -triplet projection operators are given by

$$\hat{\mathbb{P}}_{(\Lambda\Lambda)}^{(1\text{S}_0)} = -\frac{i}{2}\sigma_2, \quad \hat{\mathbb{P}}_{(\Lambda T)}^{(1\text{S}_0)} = -\frac{i}{\sqrt{2}}\sigma_2,$$

and

$$\hat{\mathbb{P}}_{(\Lambda T)_j}^{(3\text{S}_1)} = -\frac{i}{\sqrt{2}}\sigma_2\sigma_j, \quad (7)$$

respectively, with σ_j ($j = 1, 2, 3$) being the Pauli spin matrices. In the above equations $v^{\mu} = (1, \mathbf{0})$ is the velocity four-vector, and the couplings $y_{0,1,s}$ are two-body contact interactions between the respective dimer and their elementary constituent fields. Adopting to the power-counting scheme for the contact interactions, introduced in Refs. [20–22] particular to finely tuned systems, these LO couplings are easily fixed as [38]

$$y_0 = y_1 = \sqrt{\frac{2\pi}{\mu_{\Lambda T}}} \quad \text{and} \quad y_s = \sqrt{\frac{4\pi}{M_{\Lambda}}}, \quad (8)$$

with $\mu_{\Lambda T}$ being the reduced mass of the ΛT two-body subsystem, viz. one of the bound mirror states (${}_{\Lambda}^4\text{H}$, ${}_{\Lambda}^4\text{He}$). The ellipses in all the above formulas are used to denote subleading order terms containing four or higher derivative operators that do not contribute in our LO EFT analysis. For pedagogical reasons a brief description of the one- and two-body non-relativistic propagators used in the construction of the three-body integral equations is presented in the Appendix.

Finally, as demonstrated later in this section, since these three-body systems are found to exhibit RG limit cycle behavior, the set of coupled integral equations [cf. Eqns. (9) and (10)] becomes ill-defined in the asymptotic UV limit, and a regulator, say, in the form of a sharp momentum cut-off Λ_c must be introduced to obtain meaningful results. In that case, the basic tenet of the EFT [24] demands the introduction of non-derivatively coupled LO counterterms corresponding to the open elastic channels to renormalize the *artificial* scale (Λ_c) dependence in the integral equations. For the $\Lambda\Lambda T$ system

($J = 1/2, I = 1/2$), there are two equivalent choices for the sub-system spin rearrangements that determine the three-body elastic channels, namely, $u_0\Lambda \rightarrow u_0\Lambda$ (denoting as “type-A”), and $u_1\Lambda \rightarrow u_1\Lambda$ (denoting as “type-

B”). With the type-A or type-B choice as the elastic channel, the three-body counterterm Lagrangian is given either as

$$\mathcal{L}_{3\text{-body}}^{(A)} = -\frac{g_3^{(A)}(\Lambda_c)}{\Lambda_c^2} \left[-\frac{M_T y_0^2}{2} (u_0\Lambda)^\dagger (u_0\Lambda) + \frac{M_T y_0 y_1}{2} (u_0\Lambda)^\dagger (\mathbf{u}_1 \cdot \boldsymbol{\sigma}\Lambda) - \frac{M_\Lambda y_s y_0}{\sqrt{2}} (u_0\Lambda)^\dagger (u_s T) + \text{h.c.} \right], \quad (9)$$

or,

$$\mathcal{L}_{3\text{-body}}^{(B)} = -\frac{g_3^{(B)}(\Lambda_c)}{\Lambda_c^2} \left[\frac{M_T y_1^2}{6} (\mathbf{u}_1 \cdot \boldsymbol{\sigma}\Lambda)^\dagger (\mathbf{u}_1 \cdot \boldsymbol{\sigma}\Lambda) + \frac{M_T y_0 y_1}{2} (\mathbf{u}_1 \cdot \boldsymbol{\sigma}\Lambda)^\dagger (u_0\Lambda) - \frac{M_\Lambda y_s y_1}{\sqrt{2}} (\mathbf{u}_1 \cdot \boldsymbol{\sigma}\Lambda)^\dagger (u_s T) + \text{h.c.} \right]. \quad (10)$$

The scale dependent three-body running couplings $g_3^{(A,B)}(\Lambda_c)$ which are used to absorb the scale dependence of the integral equations are *a priori* undetermined in the EFT. Hence they must be phenomenologically fixed from essential three-body data. A typical signature that Efimov physics [26, 31] is manifest in the three-body system is that the RG behavior of the three-body couplings $g_3^{(A,B)}$ displays a characteristic quasi-log cyclic periodicity as a function of the regulator scale $\Lambda_c \ll \infty$. As originally suggested by Wilson [39], this unambiguously implies the onset of an RG limit cycle. Here we note that exact universality demands both three-body couplings to be identical which in principle should not depend on the details of the two-body sub-systems. However, in practice, certain nominal qualitative differences indeed appear in the estimation of these scale dependence couplings, as seen in our results presented in the next section. This is primarily a result of the specific choice of the renormalization schemes we have adopted in the treatments of the type-A and type-B integral equations (see discussion in footnote (1) in the next subsection.) However, such differences do not have any significant influence on the qualitative nature of the conclusions of this work.

B. Integral Equations

In figs. 1 and 2, we display the Feynman diagrams contributing to the S-wave elastic processes,

namely, $\Lambda u_0 \rightarrow \Lambda u_0$ (type-A) and $\Lambda u_1 \rightarrow T u_1$ (type-B), in terms of the *half-off-shell* S-wave projected amplitudes, $T_a^{(A,B)}(p, k; E)$, $T_b^{(A,B)}(p, k; E)$ and $T_c^{(A,B)}(p, k; E)$. While $T_a^{(A,B)}(p, k; E)$ denotes the elastic amplitudes, $T_b^{(A,B)}(p, k; E)$ and $T_c^{(A,B)}(p, k; E)$ are the amplitudes for the inelastic processes, $u_{0,1}\Lambda \rightarrow u_{1,0}\Lambda$ and $u_{0,1}\Lambda \rightarrow u_s\Lambda$, respectively. Here k (p) is the relative on-shell (off-shell) three-body center-of-mass momentum for the $u_{0,1} - \Lambda$ scattering processes in the initial (final) states, and $E = \mathcal{E}_{2(s,t)}^{thr} + k^2/(2\mu_{\Lambda(\Lambda T)})$ is the total center-of-mass kinetic energy measured with respect to the spin-singlet ($J^P = 0^+$) and spin-triplet ($J^P = 1^+$) *particle-dimer breakup* thresholds, $\mathcal{E}_{2(s,t)}^{thr} = -\gamma_{\Lambda T}^2/(2\mu_{\Lambda T})$. In other words, for each $\Lambda\Lambda T$ three-body system, there exists two particle-dimer thresholds, viz. the deeper $\Lambda + u_0$ breakup threshold $\mathcal{E}_{2(s)}^{thr}$ and the shallower $\Lambda + u_1$ breakup threshold $\mathcal{E}_{2(t)}^{thr}$ (cf. discussions in Sec. III.) Here $\gamma_{\Lambda T} \equiv \gamma_{0,1}$ are the binding momenta of spin-singlet and spin-triplet states of the ΛT two-body subsystems, and $\mu_{\Lambda T} = M_\Lambda M_T/(M_\Lambda + M_T)$ and $\mu_{\Lambda(\Lambda T)} = M_\Lambda(M_\Lambda + M_T)/(2M_\Lambda + M_T)$ are the reduced masses of the ΛT two-body subsystem and $\Lambda - (\Lambda T)$ three-body system, respectively. Using standard Feynman rules, the S-wave projected amplitudes for the different channels can be easily worked out. With the type-A or type-B choice as the elastic channel, the coupled integral equations is given either by [40–43]

$$T_a^{(A)}(p, k; E) = -\frac{1}{2}(y_0^2 M_T) \mathcal{K}_{(a)}^A(p, k; E) + \frac{M_T}{\mu_{\Lambda T}} \int_0^{\Lambda_c} \frac{dq q^2}{2\pi} \mathcal{K}_{(a)}^A(p, q, \Lambda_c; E) \mathcal{D}_0(q, E) T_a^{(A)}(q, k; E) \\ - \frac{y_0 \sqrt{3} M_T}{y_1 \mu_{\Lambda T}} \int_0^{\Lambda_c} \frac{dq q^2}{2\pi} \mathcal{K}_{(a)}^A(E; p, q) \mathcal{D}_1(q, E) T_b^{(A)}(q, k; E) + \frac{y_0 \sqrt{8}}{y_s} \int_0^{\Lambda_c} \frac{dq q^2}{2\pi} \mathcal{K}_{(b2)}^A(p, q; E) \mathcal{D}_s(q, E) T_c^{(A)}(q, k; E),$$

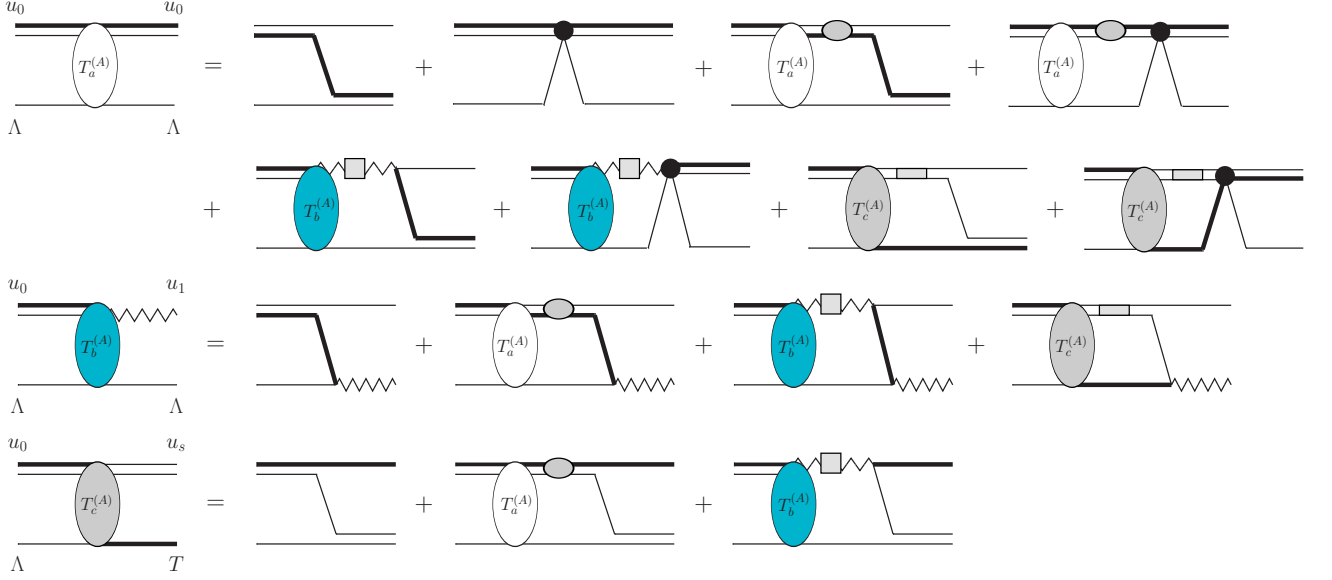


FIG. 1. Feynman diagrams for the coupled channel integral equations, with $u_0\Lambda \rightarrow u_0\Lambda$ (type-A) choice as the elastic channel. The thin (thick) lines denote the Λ -hyperon (core $T \equiv t, h$) field propagators. The double lines denote the renormalized propagators for the spin-singlet dimer fields $u_{0,s}$, and the zigzag lines denote the renormalized propagators for the spin-triplet dimer field u_1 . The dark filled circles denote the leading order three-body contact interactions, while the square, oval, and rectangular grey blobs represent dressings of the dimer propagators with resummed loops (see Appendix).

$$\begin{aligned}
T_b^{(A)}(p, k; E) &= \frac{\sqrt{3}}{2}(y_0 y_1 M_T) K_{(a)}(p, k; E) - \frac{y_1 \sqrt{3} M_T}{y_0 \mu_{\Lambda T}} \int_0^{\Lambda_c} \frac{dq q^2}{2\pi} K_{(a)}(p, q; E) \mathcal{D}_0(q, E) T_a^{(A)}(q, k; E) \\
&\quad - \frac{M_T}{\mu_{\Lambda T}} \int_0^{\Lambda_c} \frac{dq q^2}{2\pi} K_{(a)}(p, q; E) \mathcal{D}_1(q, E) T_b^{(A)}(q, k; E) + \frac{y_1 \sqrt{24}}{y_s} \int_0^{\Lambda_c} \frac{dq q^2}{2\pi} K_{(b2)}(p, q; E) \mathcal{D}_s(q, E) T_c^{(A)}(q, k; E), \\
T_c^{(A)}(p, k; E) &= -\frac{1}{\sqrt{2}}(y_0 y_s M_\Lambda) K_{(b1)}(p, k; E) + \frac{y_s \sqrt{2} M_\Lambda}{y_0 \mu_{\Lambda T}} \int_0^{\Lambda_c} \frac{dq q^2}{2\pi} K_{(b1)}(p, q; E) \mathcal{D}_0(q, E) T_a^{(A)}(q, k; E) \\
&\quad + \frac{y_s \sqrt{6} M_\Lambda}{y_1 \mu_{\Lambda T}} \int_0^{\Lambda_c} \frac{dq q^2}{2\pi} K_{(b1)}(p, q; E) \mathcal{D}_1(q, E) T_b^{(A)}(q, k; E), \tag{11}
\end{aligned}$$

or,

$$\begin{aligned}
T_a^{(B)}(p, k; E) &= \frac{1}{2}(y_1^2 M_T) \mathcal{K}_{(a)}^B(p, k; E) - \frac{M_T}{\mu_{\Lambda T}} \int_0^{\Lambda_c} \frac{dq q^2}{2\pi} \mathcal{K}_{(a)}^B(p, q, \Lambda_c; E) \mathcal{D}_1(q, E) T_a^{(B)}(q, k; E) \\
&\quad - \frac{y_1 \sqrt{3} M_T}{y_0 \mu_{\Lambda T}} \int_0^{\Lambda_c} \frac{dq q^2}{2\pi} \mathcal{K}_{(a)}^B(p, q; E) \mathcal{D}_0(q, E) T_b^{(B)}(q, k; E) + \frac{y_1 \sqrt{24}}{y_s} \int_0^{\Lambda_c} \frac{dq q^2}{2\pi} \mathcal{K}_{(b2)}^B(p, q; E) \mathcal{D}_s(q, E) T_c^{(B)}(q, k; E), \\
T_b^{(B)}(p, k; E) &= \frac{\sqrt{3}}{2}(y_1 y_0 M_T) K_{(a)}(p, k; E) - \frac{y_0 \sqrt{3} M_T}{y_1 \mu_{\Lambda T}} \int_0^{\Lambda_c} \frac{dq q^2}{2\pi} K_{(a)}(p, q; E) \mathcal{D}_1(q, E) T_a^{(B)}(q, k; E) \\
&\quad + \frac{M_T}{\mu_{\Lambda T}} \int_0^{\Lambda_c} \frac{dq q^2}{2\pi} K_{(a)}(p, q; E) \mathcal{D}_0(q, E) T_b^{(B)}(q, k; E) + \frac{y_0 \sqrt{8}}{y_s} \int_0^{\Lambda_c} \frac{dq q^2}{2\pi} K_{(b2)}(p, q; E) \mathcal{D}_s(q, E) T_c^{(B)}(q, k; E), \\
T_c^{(B)}(p, k; E) &= -\sqrt{\frac{3}{2}}(y_1 y_s M_\Lambda) K_{(b1)}(p, k; E) + \frac{y_s \sqrt{6} M_\Lambda}{y_1 \mu_{\Lambda T}} \int_0^{\Lambda_c} \frac{dq q^2}{2\pi} K_{(b1)}(p, q; E) \mathcal{D}_1(q, E) T_a^{(B)}(q, k; E) \\
&\quad + \frac{y_s \sqrt{2} M_\Lambda}{y_0 \mu_{\Lambda T}} \int_0^{\Lambda_c} \frac{dq q^2}{2\pi} K_{(b1)}(p, q; E) \mathcal{D}_0(q, E) T_b^{(B)}(q, k; E), \tag{12}
\end{aligned}$$

where the two-body couplings $y_{0,1,s}$ are determined using Eq. (8), and the energies, $E \rightarrow E_{A,B} = \mathcal{E}_{2(s,t)}^{thr} +$

$k^2/(2\mu_{\Lambda(\Lambda T)})$ are measured with respect to the $\Lambda + u_{0,1}$

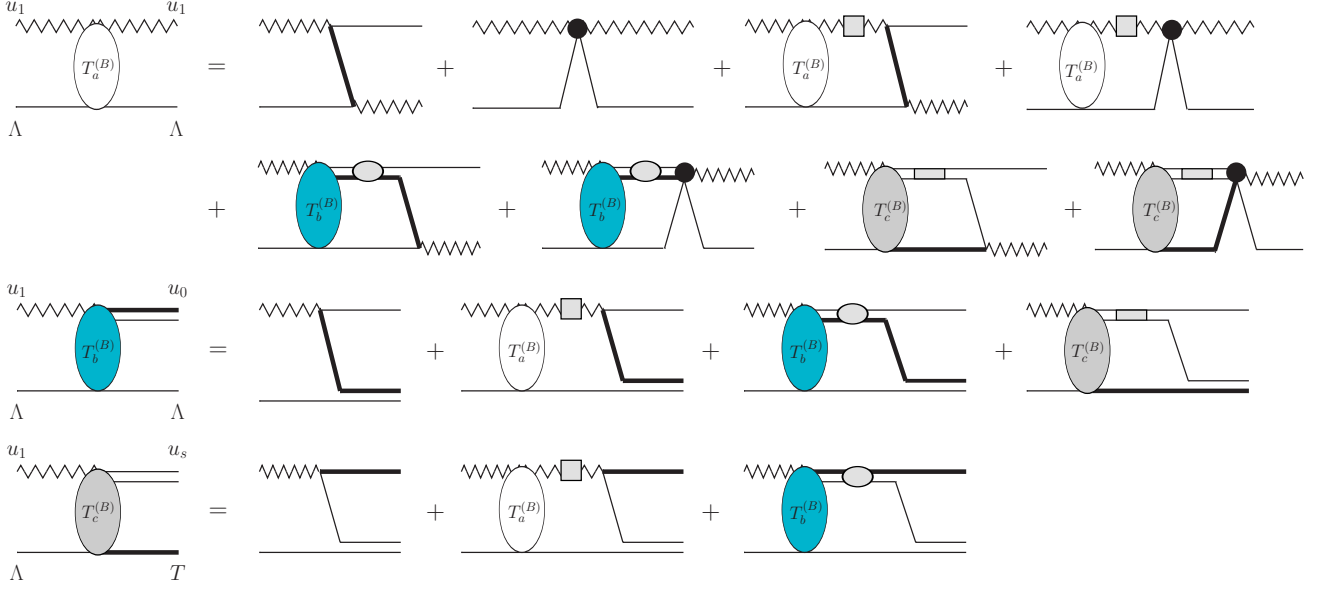


FIG. 2. Feynman diagrams for the coupled channel integral equations, with $u_1 \Lambda \rightarrow u_1 \Lambda$ (type-B) choice for the elastic channel. The thin (thick) lines denote the Λ -hyperon (core $T \equiv t, h$) field propagators. The double lines denote the renormalized propagators for the spin-singlet dimer fields $u_{0,s}$, and the zigzag lines denote the renormalized propagators for the spin-triplet dimer field u_1 . The dark filled circles denote the leading order three-body contact interactions, while the square, oval, and rectangular grey blobs represent dressings of the dimer propagators with resummed loops (see Appendix).

breakup thresholds, $\mathcal{E}_{2(s,t)}^{thr} = -\gamma_{0,1}^2/(2\mu_{\Lambda T})$. The S-wave projected two-point Green's functions (cf. Eq. (33) in the Appendix), namely,

$$\begin{aligned} \mathcal{D}_0(q, E) &= \frac{1}{\gamma_0 - \sqrt{q^2 \frac{\mu_{\Lambda T}}{\mu_{\Lambda(\Lambda T)}} - 2\mu_{\Lambda T} E - i\eta - i\eta}}, \\ \mathcal{D}_1(q, E) &= \frac{1}{\gamma_1 - \sqrt{q^2 \frac{\mu_{\Lambda T}}{\mu_{\Lambda(\Lambda T)}} - 2\mu_{\Lambda T} E - i\eta - i\eta}}, \\ \mathcal{D}_s(q, E) &= \frac{1}{\frac{1}{a_{\Lambda\Lambda}} - \sqrt{q^2 \frac{M_\Lambda}{2\mu_{T(\Lambda\Lambda)}} - M_\Lambda E - i\eta - i\eta}}, \end{aligned} \quad (13)$$

contain the contributions of the $u_{0,1,s}$ intermediate dimer states, with $\mu_{T(\Lambda\Lambda)} = (2M_\Lambda M_T)/(2M_\Lambda + M_T)$, the reduced mass of the $T - (\Lambda\Lambda)$ three-body system. The T -exchange interaction kernel $K_{(a)}$, and the two possible Λ -exchange interaction kernels, namely, $K_{(b1)}$ and $K_{(b2)}$, can be written as

$$K_{(a)}(p, \kappa; E) = \frac{1}{2p\kappa} \ln \left[\frac{p^2 + \kappa^2 + \frac{2\mu_{\Lambda T}}{M_T} p\kappa - 2\mu_{\Lambda T} E}{p^2 + \kappa^2 - \frac{2\mu_{\Lambda T}}{M_T} p\kappa - 2\mu_{\Lambda T} E} \right],$$

and

$$\begin{aligned} K_{(b1)}(p, \kappa; E) &= \frac{1}{2p\kappa} \ln \left[\frac{\frac{M_\Lambda}{2\mu_{\Lambda T}} p^2 + \kappa^2 + p\kappa - M_\Lambda E}{\frac{M_\Lambda}{2\mu_{\Lambda T}} p^2 + \kappa^2 - p\kappa - M_\Lambda E} \right], \\ K_{(b2)}(p, \kappa; E) &= \frac{1}{2p\kappa} \ln \left[\frac{p^2 + \frac{M_\Lambda}{2\mu_{\Lambda T}} \kappa^2 + p\kappa - M_\Lambda E}{p^2 + \frac{M_\Lambda}{2\mu_{\Lambda T}} \kappa^2 - p\kappa - M_\Lambda E} \right], \end{aligned} \quad (14)$$

respectively, where the generic momentum $\kappa = k(q)$ denotes the on-shell (loop) momenta. The inclusion of the cut-off dependent three-body contact couplings $g_3^{(A,B)}(\Lambda_c)$ modifies the one-particle exchange interaction kernels, $K_{(a)}$ and $K_{(b2)}$, in the respective elastic channels as¹:

$$\begin{aligned} \mathcal{K}_{(a)}^{A,B}(p, \kappa, \Lambda_c; E) &= \left[K_{(a)}(p, \kappa; E) - \frac{g_3^{(A,B)}(\Lambda_c^2)}{\Lambda_c^2} \right], \\ \mathcal{K}_{(b2)}^{A,B}(p, \kappa, \Lambda_c; E) &= \left[K_{(b2)}(p, \kappa; E) - \frac{g_3^{(A,B)}(\Lambda_c^2)}{\Lambda_c^2} \right] \end{aligned} \quad (15)$$

¹ It must be pointed out that in this work we used a minimal prescription of introducing the scale dependent three-body couplings only in the elastic channels. In general, the most systematic method of renormalization is to include them in all the inelastic channels as well, e.g., as pursued in Ref. [7, 32]. In the present case we find that the latter method in these systems leads to certain uncontrollable numerical instabilities in determining the limit cycle behaviors of $g_3^{(A,B)}(\Lambda_c)$, perhaps due to the simultaneous admixture of negative $\Lambda\Lambda$ and positive ΛT two-body scattering lengths. Hence, we resort to the former simplistic prescription. Either way, since these scale dependent couplings are *a priori* unknown and needed to be fixed phenomenologically during numerical evaluations, the three-body couplings in the different channels effectively get renormalized with the general qualitative features in the investigation of three-body bound states, e.g., the quasi-periodicity of the RG limit cycle obtained from the integral equations, mostly remaining unaffected.

C. Three-body Scattering Lengths

The coupled integral equations displayed in the previous subsection must be renormalized and then solved numerically to yield predictions for the $\Lambda\Lambda T$ three-body scattering amplitudes. For a given on-shell relative momentum $k = |\mathbf{k}|$ and three-body center-of-mass kinetic energy E , the kinematical scattering domain lies between the particle-dimer breakup thresholds $\mathcal{E}_{2(s,t)}^{thr}$ and the *three-particle breakup* threshold, i.e., $\mathcal{E}_{2(s,t)}^{thr} < E < 0$. In contrast to the kinematical domain of three-body bound states ($E < \mathcal{E}_{2(s,t)}^{thr}$ and imaginary k) which is free of singularities, the integral equations in the scattering domain develop singularities associated with poles of the ΛT dimer propagators $\mathcal{D}_{0,1}(q, E)$ for certain values of the loop momenta q . For type-A integral equa-

tions the only poles are that of the propagator $\mathcal{D}_0(q, E)$ at $q = k$, while for the type-B integral equations both the ΛT dimer propagators develop poles; $\mathcal{D}_1(q, E)$ has a pole at $q = k$ and $\mathcal{D}_0(q, E)$ has a pole at $q = \sqrt{k^2 + (\gamma_0^2 - \gamma_1^2)(\mu_{\Lambda(\Lambda T)}/\mu_{\Lambda T})}$. To avoid these poles, a *principal value* prescription must be used in the appropriate loop integrals to extract the three-body scattering amplitudes. Furthermore, it is numerically advantageous to express the otherwise complex valued integral equation below the three-particle breakup threshold in terms of the real valued renormalized K-matrix elements $\mathbb{K}_{a,b,c}^{(A,B)}(p, k; E)$ for the respective choice of the elastic processes, namely, $u_{(0,1)}\Lambda \rightarrow u_{(0,1)}\Lambda$. To this end we display the principal value prescription modified renormalized integral equations:

$$\begin{aligned}
\mathbb{K}_a^{(A)}(p, k; E) &= -\frac{M_T}{4\mu_{\Lambda T}} \mathcal{M}_{(a)}^{A(0)}(p, k; E) - \frac{M_T}{2\pi\mu_{\Lambda T}} \mathcal{P} \int_0^{\Lambda_c} dq \mathcal{M}_{(a)}^{A(0)}(p, q, \Lambda_c; E) \frac{q^2}{q^2 - k^2} \mathbb{K}_a^{(A)}(q, k; E) \\
&+ \frac{\sqrt{3}M_T y_0}{2\pi\mu_{\Lambda T} y_1} \int_0^{\Lambda_c} dq \mathcal{M}_{(a)}^{A(0)}(p, q, \Lambda_c; E) \frac{q^2}{q^2 - k^2 + \frac{\mu_{\Lambda(\Lambda T)}}{\mu_{\Lambda T}}(\gamma_0^2 - \gamma_1^2)} \mathbb{K}_b^{(A)}(q, k; E) \\
&- \frac{\sqrt{2}}{\pi} \frac{y_0}{y_s} \mathcal{P} \int_0^{\Lambda_c} dq \mathcal{M}_{(b2)}^{A(0)}(p, q, \Lambda_c; E) \frac{q^2}{q^2 - k^2} \mathbb{K}_c^{(A)}(q, k; E), \\
\mathbb{K}_b^{(A)}(p, k; E) &= \frac{\sqrt{3}M_T y_1}{4\mu_{\Lambda T} y_0} M_{(a)}^{(1)}(p, k; E) + \frac{\sqrt{3}M_T y_1}{2\pi\mu_{\Lambda T} y_0} \mathcal{P} \int_0^{\Lambda_c} dq M_{(a)}^{(1)}(p, q; E) \frac{q^2}{q^2 - k^2} \mathbb{K}_a^{(A)}(q, k; E) \\
&+ \frac{M_T}{2\pi\mu_{\Lambda T}} \int_0^{\Lambda_c} dq M_{(a)}^{(1)}(p, q; E) \frac{q^2}{q^2 - k^2 + \frac{\mu_{\Lambda(\Lambda T)}}{\mu_{\Lambda T}}(\gamma_0^2 - \gamma_1^2)} \mathbb{K}_b^{(A)}(q, k; E) \\
&- \frac{\sqrt{6}}{\pi} \frac{y_1}{y_s} \mathcal{P} \int_0^{\Lambda_c} dq M_{(b2)}^{(1)}(p, q; E) \frac{q^2}{q^2 - k^2} \mathbb{K}_c^{(A)}(q, k; E), \\
\mathbb{K}_c^{(A)}(p, k; E) &= \frac{M_\Lambda}{2\sqrt{2}\mu_{\Lambda T} y_0} M_{(b1)}(p, k; E) + \frac{M_\Lambda}{\sqrt{2}\pi\mu_{\Lambda T} y_0} \mathcal{P} \int_0^{\Lambda_c} dq M_{(b1)}(p, q; E) \frac{q^2}{q^2 - k^2} \mathbb{K}_a^{(A)}(q, k; E) \\
&+ \sqrt{\frac{3}{2}} \frac{M_\Lambda}{\pi\mu_{\Lambda T} y_1} \int_0^{\Lambda_c} dq M_{(b1)}(p, q; E) \frac{q^2}{q^2 - k^2 + \frac{\mu_{\Lambda(\Lambda T)}}{\mu_{\Lambda T}}(\gamma_0^2 - \gamma_1^2)} \mathbb{K}_b^{(A)}(q, k; E),
\end{aligned} \tag{16}$$

for the type-A elastic channel with $E = E_A = \mathcal{E}_{2(s)}^{thr} + k^2/(2\mu_{\Lambda(\Lambda T)})$, and

$$\begin{aligned}
\mathbb{K}_a^{(B)}(p, k; E) &= \frac{M_T}{4\mu_{\Lambda T}} \mathcal{M}_{(a)}^{B(1)}(p, k; E) + \frac{M_T}{2\pi\mu_{\Lambda T}} \mathcal{P} \int_0^{\Lambda_c} dq \mathcal{M}_{(a)}^{B(1)}(p, q, \Lambda_c; E) \frac{q^2}{q^2 - k^2} \mathbb{K}_a^{(B)}(q, k; E) \\
&+ \frac{\sqrt{3}M_T y_1}{2\pi\mu_{\Lambda T} y_0} \mathcal{P} \int_0^{\Lambda_c} dq \mathcal{M}_{(a)}^{A(1)}(p, q, \Lambda_c; E) \frac{q^2}{q^2 - k^2 - \frac{\mu_{\Lambda(\Lambda T)}}{\mu_{\Lambda T}}(\gamma_0^2 - \gamma_1^2)} \mathbb{K}_b^{(B)}(q, k; E) \\
&- \frac{\sqrt{6}}{\pi} \frac{y_1}{y_s} \mathcal{P} \int_0^{\Lambda_c} dq \mathcal{M}_{(b2)}^{A(1)}(p, q, \Lambda_c; E) \frac{q^2}{q^2 - k^2} \mathbb{K}_c^{(B)}(q, k; E),
\end{aligned}$$

$$\begin{aligned}
\mathbb{K}_b^{(B)}(p, k; E) &= \frac{\sqrt{3}M_T y_0}{4\mu_{\Lambda T} y_1} M_{(a)}^{(0)}(p, k; E) + \frac{\sqrt{3}M_T y_0}{2\pi\mu_{\Lambda T} y_1} \mathcal{P} \int_0^{\Lambda_c} dq M_{(a)}^{(0)}(p, q; E) \frac{q^2}{q^2 - k^2} \mathbb{K}_a^{(B)}(q, k; E) \\
&\quad - \frac{M_T}{2\pi\mu_{\Lambda T}} \mathcal{P} \int_0^{\Lambda_c} dq M_{(a)}^{(0)}(p, q; E) \frac{q^2}{q^2 - k^2 - \frac{\mu_{\Lambda(\Lambda T)}}{\mu_{\Lambda T}}(\gamma_0^2 - \gamma_1^2)} \mathbb{K}_b^{(B)}(q, k; E) \\
&\quad - \frac{\sqrt{2}}{\pi} \frac{y_0}{y_s} \mathcal{P} \int_0^{\Lambda_c} dq M_{(b2)}^{(0)}(p, q; E) \frac{q^2}{q^2 - k^2} \mathbb{K}_c^{(B)}(q, k; E) , \\
\mathbb{K}_c^{(B)}(p, k; E) &= \frac{\sqrt{3}M_\Lambda y_s}{2\sqrt{2}\mu_{\Lambda T} y_1} M_{(b1)}(p, k; E) + \sqrt{\frac{3}{2}} \frac{M_\Lambda y_s}{\pi\mu_{\Lambda T} y_1} \mathcal{P} \int_0^{\Lambda_c} dq M_{(b1)}(p, q; E) \frac{q^2}{q^2 - k^2} \mathbb{K}_a^{(B)}(q, k; E) \\
&\quad + \frac{M_\Lambda y_s}{\sqrt{2}\pi\mu_{\Lambda T} y_0} \mathcal{P} \int_0^{\Lambda_c} dq M_{(b1)}(p, q; E) \frac{q^2}{q^2 - k^2 - \frac{\mu_{\Lambda(\Lambda T)}}{\mu_{\Lambda T}}(\gamma_0^2 - \gamma_1^2)} \mathbb{K}_b^{(B)}(q, k; E) ,
\end{aligned} \tag{17}$$

for the type-B elastic channel with $E = E_B = \mathcal{E}_{2(t)}^{thr} + k^2/(2\mu_{\Lambda(\Lambda T)})$. The symbol ‘‘ \mathcal{P} ’’ stands for a principal value integral which involves rewriting the complex dimer propagators with $i\eta$ prescription in terms of the corresponding real valued propagators, namely,

$$\frac{1}{q^2 - k^2 - i\eta} = \mathcal{P} \frac{1}{q^2 - k^2} + i\pi\delta(q^2 - k^2) ,$$

and

$$\begin{aligned}
&\frac{1}{q^2 - k^2 - \frac{\mu_{\Lambda(\Lambda T)}}{\mu_{\Lambda T}}(\gamma_0^2 - \gamma_1^2) - i\eta} \\
&= \mathcal{P} \frac{1}{q^2 - k^2 - \frac{\mu_{\Lambda(\Lambda T)}}{\mu_{\Lambda T}}(\gamma_0^2 - \gamma_1^2)} \\
&\quad + i\pi\delta\left(q^2 - k^2 - \frac{\mu_{\Lambda(\Lambda T)}}{\mu_{\Lambda T}}(\gamma_0^2 - \gamma_1^2)\right) .
\end{aligned}$$

The S-wave projected Λ - and T -exchange interactions kernels in this case are rewritten as:

$$\begin{aligned}
M_{(a)}^{(0,1)}(p, \kappa; E) &= \left(\frac{\mu_{\Lambda(\Lambda T)}}{\mu_{\Lambda T}}\right) K_{(a)}(p, \kappa; E) \\
&\quad \times \left(\gamma_{0,1} + \sqrt{p^2 \frac{\mu_{\Lambda T}}{\mu_{\Lambda(\Lambda T)}} - 2\mu_{\Lambda T} E}\right) , \\
M_{(b1)}(p, \kappa; E) &= K_{(b1)} \left(\frac{p^2 - k^2}{\frac{1}{a_{\Lambda\Lambda}} - \sqrt{q^2 \frac{M_\Lambda}{2\mu_{T(\Lambda\Lambda)}}} - M_\Lambda E}\right) , \\
M_{(b2)}^{(0,1)}(p, \kappa; E) &= \left(\frac{\mu_{\Lambda(\Lambda T)}}{\mu_{\Lambda T}}\right) K_{(b2)}(p, \kappa; E) \\
&\quad \times \left(\gamma_{0,1} + \sqrt{p^2 \frac{\mu_{\Lambda T}}{\mu_{\Lambda(\Lambda T)}} - 2\mu_{\Lambda T} E}\right) ,
\end{aligned} \tag{18}$$

and the corresponding three-body force modified Λ_c dependent kernels needed are:

$$\begin{aligned}
\mathcal{M}_{(a)}^{A,B(0,1)}(p, \kappa, \Lambda_c; E) &= \left(\frac{\mu_{\Lambda(\Lambda T)}}{\mu_{\Lambda T}}\right) \mathcal{K}_{(a)}^{A,B}(p, \kappa, \Lambda_c; E) \\
&\quad \times \left(\gamma_{0,1} + \sqrt{p^2 \frac{\mu_{\Lambda T}}{\mu_{\Lambda(\Lambda T)}} - 2\mu_{\Lambda T} E}\right) , \\
\mathcal{M}_{(b2)}^{A,B(0,1)}(p, \kappa, \Lambda_c; E) &= \left(\frac{\mu_{\Lambda(\Lambda T)}}{\mu_{\Lambda T}}\right) \mathcal{K}_{(b2)}^{A,B}(p, \kappa, \Lambda_c; E) \\
&\quad \times \left(\gamma_{0,1} + \sqrt{p^2 \frac{\mu_{\Lambda T}}{\mu_{\Lambda(\Lambda T)}} - 2\mu_{\Lambda T} E}\right) ,
\end{aligned} \tag{19}$$

where $\kappa = k(q)$ is the on-shell (loop) momentum. In the above integral equations, the unrenormalized complex amplitudes $T_a^{(A,B)}(p, k; E)$ are related to the renormalized real-valued K-matrix elements $\mathbb{K}_{a,b,c}^{(A,B)}(p, k; E)$ by the following relations:

$$\begin{aligned}
\frac{\mathbb{K}_a^{(A)}(p, k; E)}{k^2 - p^2} &= \left(\frac{\mu_{\Lambda T}}{4\pi\gamma_0}\right) \frac{\sqrt{Z_0} T_a^{(A)}(p, k; E) \sqrt{Z_0}}{\gamma_0 - \sqrt{q^2 \frac{\mu_{\Lambda T}}{\mu_{\Lambda(\Lambda T)}}} - 2\mu_{\Lambda T} E} , \\
\frac{\mathbb{K}_b^{(A)}(p, k; E)}{k^2 - p^2 + \frac{\mu_{\Lambda(\Lambda T)}}{\mu_{\Lambda T}}(\gamma_0^2 - \gamma_1^2)} &= \left(\frac{\mu_{\Lambda T}}{4\pi\gamma_0}\right) \frac{\sqrt{Z_0} T_b^{(A)}(p, k; E) \sqrt{Z_0}}{\gamma_1 - \sqrt{q^2 \frac{\mu_{\Lambda T}}{\mu_{\Lambda(\Lambda T)}}} - 2\mu_{\Lambda T} E} , \\
\frac{\mathbb{K}_c^{(A)}(p, k; E)}{k^2 - p^2} &= \left(\frac{\mu_{\Lambda T}}{4\pi\gamma_0}\right) \frac{\sqrt{Z_0} T_c^{(A)}(p, k; E) \sqrt{Z_0}}{\frac{1}{a_{\Lambda\Lambda}} - \sqrt{q^2 \frac{M_\Lambda}{2\mu_{T(\Lambda\Lambda)}}} - M_\Lambda E} ,
\end{aligned} \tag{20}$$

for the type-A amplitudes, and

$$\frac{\mathbb{K}_a^{(B)}(p, k; E)}{k^2 - p^2} = \left(\frac{\mu_{\Lambda T}}{4\pi\gamma_1}\right) \frac{\sqrt{Z_1} T_a^{(B)}(p, k; E) \sqrt{Z_1}}{\gamma_1 - \sqrt{q^2 \frac{\mu_{\Lambda T}}{\mu_{\Lambda(\Lambda T)}}} - 2\mu_{\Lambda T} E} ,$$

D. Asymptotic Bound State Analysis

$$\begin{aligned} \frac{\mathbb{K}_b^{(B)}(p, k; E)}{k^2 - p^2 - \frac{\mu_{\Lambda(\Lambda T)}}{\mu_{\Lambda T}}(\gamma_0^2 - \gamma_1^2)} &= \left(\frac{\mu_{\Lambda T}}{4\pi\gamma_1} \right) \frac{\sqrt{Z_1} T_b^{(B)}(p, k; E) \sqrt{Z_1}}{\gamma_0 - \sqrt{q^2 \frac{\mu_{\Lambda T}}{\mu_{\Lambda(\Lambda T)}} - 2\mu_{\Lambda T} E}}, \\ \frac{\mathbb{K}_c^{(B)}(p, k; E)}{k^2 - p^2} &= \left(\frac{\mu_{\Lambda T}}{4\pi\gamma_1} \right) \frac{\sqrt{Z_1} T_c^{(B)}(p, k; E) \sqrt{Z_1}}{\frac{1}{a_{\Lambda\Lambda}} - \sqrt{q^2 \frac{M_{\Lambda}}{2\mu_{T(\Lambda\Lambda)}} - M_{\Lambda} E}}, \end{aligned} \quad (21)$$

for the type-B amplitudes, where $Z_{0,1}$ are the $u_{0,1}$ -dimer wavefunction renormalization constants, defined as the residues of the renormalized dressed dimer propagators $\Delta_{0,1}(k_0, \mathbf{k})$ [cf. Eq. (33) in the Appendix]:

$$\begin{aligned} Z_0^{-1} &= \frac{d[\Delta_0^{-1}(k_0, \mathbf{0})]}{dk_0} \Big|_{k_0 = -\mathcal{B}_{\Lambda}[0^+]} = \frac{\mu_{\Lambda T}^2 y_0^2}{2\pi\gamma_0}, \\ Z_1^{-1} &= \frac{d[\Delta_1^{-1}(k_0, \mathbf{0})]}{dk_0} \Big|_{k_0 = -\mathcal{B}_{\Lambda}[1^+]} = \frac{\mu_{\Lambda T}^2 y_1^2}{2\pi\gamma_1}. \end{aligned} \quad (22)$$

Finally, the $J = 1/2$ S-wave $\Lambda\Lambda T$ scattering lengths are obtained by numerically solving the above integral equations for the renormalized on-shell elastic scattering amplitudes $\mathbb{K}_a^{(A,B)}(k, k)$, and then taking the threshold limit ($k \rightarrow 0$) according to the definition

$$a_{3(s,t)} = - \lim_{k \rightarrow 0} \mathbb{K}_a^{(A,B)}(k, k). \quad (23)$$

It is important to realize that neither of the two $\Lambda\Lambda T$ scattering lengths above, corresponding to the constituent spin-singlet and spin-triplet ΛT subsystems, can be considered as physical observables. Rather it is the effective three-body scattering length $a_{\Lambda\Lambda T}$ that may perhaps be physically extracted at low-energies from the $(2J + 1)$ -spin average S-wave elastic cross section $\sigma_{\Lambda\Lambda T}^{el}$ using the relation

$$a_{\Lambda\Lambda T} = \sqrt{\frac{1}{4} a_{3(s)}^2 + \frac{3}{4} a_{3(t)}^2}, \quad (24)$$

vis-a-vis the prescription:

$$\begin{aligned} \sigma_{\Lambda\Lambda T}^{el} &= \frac{1}{4} \sigma_{3(s)}(\text{type-A}) + \frac{3}{4} \sigma_{3(t)}(\text{type-B}); \\ a_{3(s,t)} &= \lim_{k \rightarrow 0} \sqrt{\frac{1}{4\pi} \sigma_{3(s,t)}(\text{type-A,B})}, \\ a_{\Lambda\Lambda T} &= \lim_{k \rightarrow 0} \sqrt{\frac{1}{4\pi} \sigma_{\Lambda\Lambda T}^{el}}. \end{aligned} \quad (25)$$

Having said that it must be borne in mind that there are currently no experiments that can possibly extract these scattering lengths by measuring the above elastic cross sections. The unstable nature of the Λ -hyperon poses an immense technical challenge to be used either as targets or projectiles in scattering experiments. Nevertheless, the present work demonstrates the kind of prototypical EFT analysis that may be necessary whenever such information becomes feasible from future experimental investigations.

In the investigation of three-body bound state characteristic in the $\Lambda\Lambda T$ systems, the emergence of RG limit-cycle behavior could be easily checked by studying the asymptotic UV limit of the coupled system of integral equations where the off-shell or loop momenta $q, p \sim \Lambda_c \rightarrow \infty$, and the on-shell energy and relative momenta $E, k \sim \gamma_{0,1} \sim 1/a_{\Lambda\Lambda} \ll p, q$. In this limit the inhomogeneous parts as well as the Λ_c^{-2} suppressed three-body contributions to the integral equations drop out. After suitable re-definitions of the half-off-shell amplitudes, they may be shown to scale for generic off-shell asymptotic momenta κ as $T_{a,b,c}^{(A,B)}(\kappa \rightarrow \infty) \sim \kappa^{s-1}$ (irrespective of the type-A or type-B choice for the elastic channels). Finally through a sequence of *Mellin transformations*, both sets of integral equations are reduced to a single transcendental form

$$\begin{aligned} 1 &= \left(\frac{M_T}{2\pi\mu_{\Lambda T} C_1} \right) \left[\frac{2\pi \sin[s \sin^{-1}(a/2)]}{s \cos[\pi s/2]} \right] \\ &+ \left(\frac{M_{\Lambda}}{\pi^2 \mu_{\Lambda T} C_1 C_2} \right) \left[\frac{2\pi \sin[s \cot^{-1} \sqrt{4b-1}]}{s \cos[\pi s/2]} \right]^2, \end{aligned} \quad (26)$$

where

$$\begin{aligned} a &= \frac{2\mu_{\Lambda T}}{M_T}, \quad b = \frac{M_{\Lambda}}{2\mu_{\Lambda T}}, \\ C_1 &= \sqrt{\frac{\mu_{\Lambda T}}{\mu_{\Lambda(\Lambda T)}}}, \quad C_2 = \sqrt{\frac{M_{\Lambda}}{2\mu_{T(\Lambda\Lambda)}}}. \end{aligned}$$

Solving for the exponent s in above equation yields the following imaginary values:

$$s = \pm i s_0^{\infty} \begin{cases} s_0^{\infty} = 1.03517\dots & \text{for } \Lambda_{\Lambda}^5 \text{H} \\ s_0^{\infty} = 1.03516\dots & \text{for } \Lambda_{\Lambda}^5 \text{He}. \end{cases} \quad (27)$$

The small numerical difference between the values of the asymptotic limit cycle parameter s_0^{∞} reflects their universal character with reasonably good isospin symmetry between the mirror hypernuclei ($\Lambda_{\Lambda}^5 \text{H}$, $\Lambda_{\Lambda}^5 \text{He}$). The imaginary solutions can be formally attributed to the existence of Efimov states in the unitary limit of these cluster systems and parametrize the onset of discrete scaling invariance. A detailed exposition of this kind of asymptotic analysis leading to Efimov effect is found in Ref. [26]. In the next section we present a qualitative assay of our numerical results for the non-asymptotic solutions to the integral equations and their possible implications in the low-energy domain.

III. RESULTS AND DISCUSSION

For our numerical evaluations, we use the masses of the particles as displayed in Table. I. As a comparison to our already obtained asymptotic limit cycle parameter s_0^{∞} for each mirror hypernuclei, the analogous non-asymptotic

Particle	Symbol	Mass (MeV)	Binding energy (MeV)
Λ -hyperon	Λ	1115.683	-
Triton ${}^3\text{H}$	t	2808.921	8.48
Helion ${}^3\text{He}$	h	2808.391	7.72

TABLE I. Particle data used in our calculations [44].

parameter s_0 may be obtained by studying the RG behavior of the the three-body couplings $g_3^{(A,B)}(\Lambda_c)$ for non-asymptotic kinematics. These parameters are, however, non-universal in character and sensitive to the cut-off variations. Nevertheless, it may be shown that as $\Lambda_c \rightarrow \infty$, $s_0 \rightarrow s_0^\infty$ [30]. We note that currently there is no empirical three-body information available to constraint $g_3^{(A,B)}$. Thus, we adopt a strategy similar to the earlier pursued works [27, 28, 30]. We assume that ${}_{\Lambda\Lambda}^5\text{H}$ and ${}_{\Lambda\Lambda}^5\text{He}$ already form Efimov-like bound cluster states and thereby investigate the RG of $g_3^{(A,B)}$ by choosing three sets of $\Lambda\Lambda$ separation energies² $B_{\Lambda\Lambda}$ and the S-wave $\Lambda\Lambda$ -scattering lengths $a_{\Lambda\Lambda}$, taken from the potential model analysis of Ref. [8], corresponding to ${}_{\Lambda\Lambda}^5\text{H}$ and ${}_{\Lambda\Lambda}^5\text{He}$ systems (cf. Table. II). Infact, the $\Lambda\Lambda$ scattering lengths used as input to the Feddeev-type equations in Ref. [8] correspond to several versions of Nijmegen Soft-core potential model results [33, 34].

In fig. 3, we plot the cut-off dependence of the type-A and type-B three-body couplings, $g_3^{(A,B)}(\Lambda_c)$, which displays the characteristic quasi-periodic singularities of the limit cycle behaviors associated with the successive formation of three-body bound states in the non-asymptotic domain. It is apparent that due to the reasonably good isospin symmetry between the two double- Λ mirror hypernuclei, there is little observable difference in the RG behaviors. As already pointed out, ideally the scale dependence of the type-A and type-B coupling for a given three-body system (${}_{\Lambda\Lambda}^5\text{H}$ or ${}_{\Lambda\Lambda}^5\text{He}$) should be identical.

² The double- Λ separation energy $B_{\Lambda\Lambda}$, as commonly referred to in the context of potential models, is interpreted in our EFT analysis as the three-body binding energy, $-E = B_{\Lambda\Lambda}$ obtained as one of the eigensolutions of the homogeneous part of the integral equations. Furthermore, in the potential model analysis [8] the authors have introduced an *incremental* binding energy $\Delta B_{\Lambda\Lambda}$ which is related to $B_{\Lambda\Lambda}$ (measured with respect to the $\Lambda\Lambda T$ three-particle breakup threshold) as

$$B_{\Lambda\Lambda} = 2\mathcal{B}_\Lambda^{avg} + \Delta B_{\Lambda\Lambda}, \quad (28)$$

where,

$$\mathcal{B}_\Lambda^{avg} = \frac{1}{4}\mathcal{B}_\Lambda[0^+] + \frac{3}{4}\mathcal{B}_\Lambda[1^+], \quad (29)$$

is the $(2J+1)$ *spin average* of the ΛT binding energies (also commonly termed as the Λ separation energies) over the singlet and triplet two-body level states. It must be noted here that the predicted incremental binding energies $\Delta B_{\Lambda\Lambda}$ from the Faddeev calculation analysis of ${}_{\Lambda\Lambda}^5\text{H}$ and ${}_{\Lambda\Lambda}^5\text{He}$ (cf. Table. VIII of [8]) were used in our work to obtain the corresponding binding energies $B_{\Lambda\Lambda}$ using the above relations, as displayed in Table. II. These numerical values were not explicitly quoted in Ref. [8].

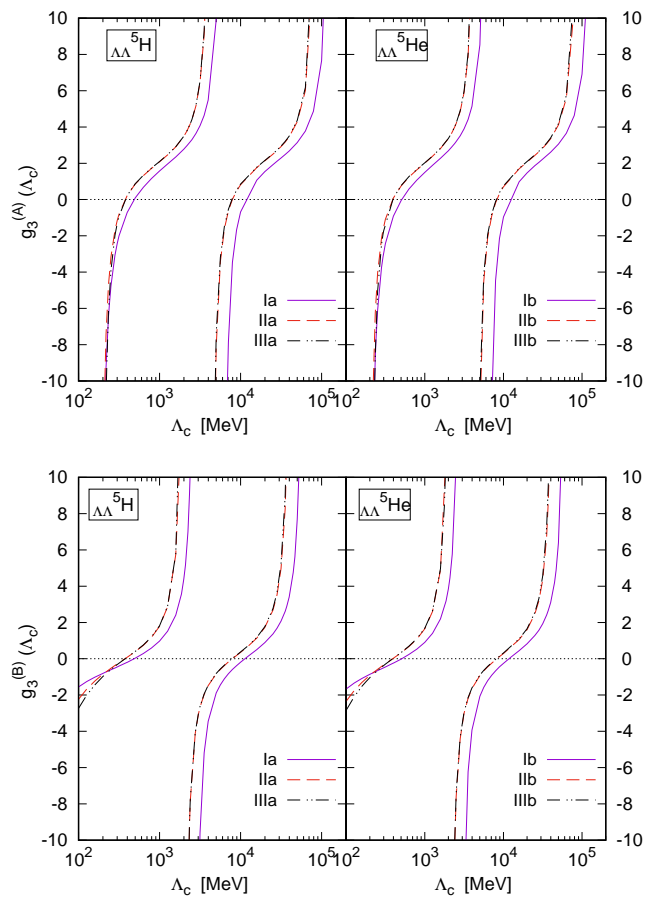


FIG. 3. The RG limit cycles of the three-body coupling $g_3^{(A,B)}(\Lambda_c)$ for the $\Lambda\Lambda T$ ($T \equiv t, h$) systems, corresponding to the mirror hypernuclei (${}_{\Lambda\Lambda}^5\text{H}$, ${}_{\Lambda\Lambda}^5\text{He}$). These results were obtained for several Nijmegen Soft-core potential model predicted $\Lambda\Lambda$ -scattering lengths $a_{\Lambda\Lambda}$, taken from Refs. [33, 34], and three-body binding energies (double- Λ separation energies) $B_{\Lambda\Lambda}$, obtained from the potential model analysis of Ref. [8] (see Table II). The upper (lower) panel corresponds to the type-A (type-B) choice of the elastic channel.

However, due to the differences in the type-A and type-B elastic channels where we choose to introduce the three-body counterterms (cf. figs. 1 and 2), we find that the type-B limit cycle curves are nominally shifted leftwards and downwards with respect to the type-A curves. Nevertheless, the scales $(\Lambda_c)_n$ at which these couplings successively vanish remain unaltered. In each case the non-asymptotic RG limit cycle parameter s_0 can be calculated using the relation

$$s_0 = \frac{\pi}{\ln \left[\frac{(\Lambda_c)_{n+1}}{(\Lambda_c)_n} \right]}; \quad n = 0, 1, 2, \dots \quad (30)$$

where $(\Lambda_c)_n$ is the momentum cut-off corresponding to the n^{th} zero of $g_3^{(A,B)}$. Using, e.g., the second ($n = 1$) and the third ($n = 2$) values of Λ_c we obtain $s_0 = \pi / \ln[(\Lambda_c)_2 / (\Lambda_c)_1] \sim 1.03$ for both the mirror hypernu-

Hypernucleus Sets	Scattering length $a_{\Lambda\Lambda}$ (fm) [33, 34]	Incremental binding energy $\Delta B_{\Lambda\Lambda}$ (MeV) [8]	$\Lambda\Lambda$ separation energy $B_{\Lambda\Lambda}$ (MeV) [8]	Critical cut-off $\Lambda_{\text{crit}}^{(n=0)}$ (MeV) (with $g_3^{(A,B)} = 0$)	Cut-off $\Lambda_{\text{pot}}^{(n=0)}$ (MeV) (with $g_3^{(A,B)} = 0$)
Ia (${}_{\Lambda\Lambda}^5\text{H}$)	-0.50 (NSC97e)	0.50	2.960	305.17	486.93
Ib (${}_{\Lambda\Lambda}^5\text{He}$)	-0.50 (NSC97e)	0.55	3.605	299.26	508.87
IIa (${}_{\Lambda\Lambda}^5\text{H}$)	-2.81 (ND)	2.11	4.570	172.63	374.35
IIb (${}_{\Lambda\Lambda}^5\text{He}$)	-2.81 (ND)	2.27	5.325	175.07	390.39
IIIa (${}_{\Lambda\Lambda}^5\text{H}$)	-10.6 (ESC00)	3.46	5.920	139.96	376.16
IIIb (${}_{\Lambda\Lambda}^5\text{He}$)	-10.6 (ESC00)	3.68	6.735	114.11	391.37

TABLE II. Three sets of evaluations of the double- Λ separation energy $B_{\Lambda\Lambda}$ for the double- Λ mirror hypernuclei (${}_{\Lambda\Lambda}^5\text{H}$, ${}_{\Lambda\Lambda}^5\text{He}$) using Eq. (28) taken Ref. [8]. In this reference, the respective incremental binding energies $\Delta B_{\Lambda\Lambda}$ were evaluated using Faddeev calculations where the $\Lambda\Lambda$ S-wave scattering lengths $a_{\Lambda\Lambda}$ predicted from several Nijmegen Soft-core potential models [33, 34] (names displayed in parentheses) were used as input. Furthermore, with the three-body interactions excluded, i.e., $g_3^{(A,B)} = 0$, the critical cut-offs, $\Lambda_c = \Lambda_{\text{crit}}^{(n=0)}$, namely, the values at which the ground states trimers for these hypernuclei appear at threshold are displayed. The last column displays our adjusted cut-off values, $\Lambda_c = \Lambda_{\text{pot}}^{(n=0)}$, which reproduce the above values of potential model separation energies $B_{\Lambda\Lambda}$ as ground state eigenenergies.

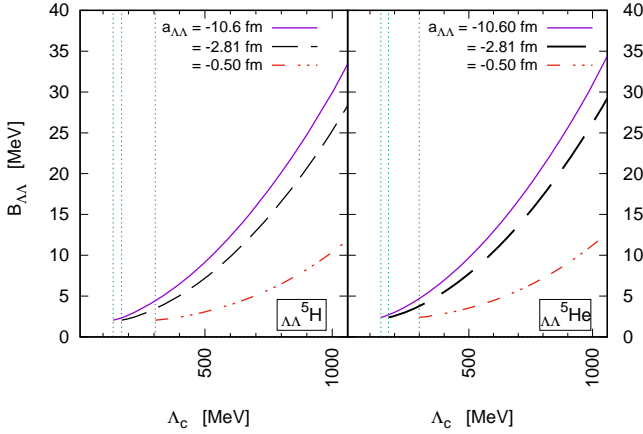


FIG. 4. The three-body binding energies (double- Λ separation energies) $B_{\Lambda\Lambda}$ corresponding to the mirror hypernuclei (${}_{\Lambda\Lambda}^5\text{H}$, ${}_{\Lambda\Lambda}^5\text{He}$) versus the cut-off scale Λ_c for different Nijmegen Soft-core potential model predicted $\Lambda\Lambda$ -scattering lengths, namely, $a_{\Lambda\Lambda} = -0.5, -2.81,$ and -10.6 fm, obtained from Refs. [33, 34]. The three-body couplings $g_3^{(A,B)}$ were excluded here. The vertical lines denote only the deeper particle-dimer breakup thresholds, namely, the $\Lambda + u_0$ thresholds for the respective hypernuclei. The plots correspond to either of type-A and type-B elastic channels.

clei, which agrees well with the asymptotic values of s_0^∞ given in Eq. (27), irrespective of the choice of the elastic channel. Moreover our s_0 values are also in good agreement with the “calibration plot” of Ref. [26] for $\exp(\pi/s_0)$ versus the mass ratio m_1/m_3 for a mass imbalanced system with $m_1 = m_2 \equiv M_\Lambda$ and $m_3 \equiv M_T \neq m_{1,2}$.

Next we report our results for the Λ_c dependence of the double- Λ separation energy $B_{\Lambda\Lambda}$ of ${}_{\Lambda\Lambda}^5\text{H}$ and ${}_{\Lambda\Lambda}^5\text{He}$ obtained by numerically solving the homogeneous parts of the two sets of integral equations [cf. Eqns. (11) and (12)], excluding the three-body contact interaction, i.e., $g_3^{(A,B)} = 0$. The same set of Nijmegen Soft-core po-

tential model predicted $\Lambda\Lambda$ -scattering lengths, namely, $a_{\Lambda\Lambda} = -0.5, -2.81,$ and -10.6 fm [33, 34] were used to obtain the results. It may be noted that both choices for the elastic channels yield the same results. As displayed in the fig. 4, the binding energy of ${}_{\Lambda\Lambda}^5\text{He}$ is found to be slightly greater than ${}_{\Lambda\Lambda}^5\text{H}$ owing to the larger binding energy of the two-body core Λh (i.e., ${}^4_\Lambda\text{H}$) compared to the Λt core (i.e., ${}^4_\Lambda\text{He}$). Evidently, in the absence of the three-body contact interactions to renormalize the integral equations, the three-body binding energies are found to be quite sensitive to the cut-off variations, which increase with increasing cut-off starting from certain threshold values, namely, the respective $\Lambda + u_0$ particle-dimer breakup thresholds $\mathcal{E}_{2(s)}^{\text{thr}}$ defined by

$$B_{\Lambda\Lambda}(\Lambda_{\text{crit}}^{(n=0)}) \equiv -\mathcal{E}_{2(s)}^{\text{thr}} = \frac{\gamma_0^2}{2\mu_{\Lambda T}}$$

$$\rightsquigarrow \mathcal{B}_\Lambda[0^+] = \begin{cases} 2.04 \text{ MeV [5]} & \text{for } {}^4_\Lambda\text{H}[0^+] \\ 2.39 \text{ MeV [5]} & \text{for } {}^4_\Lambda\text{He}[0^+]. \end{cases} \quad (31)$$

Here $\Lambda_c = \Lambda_{\text{crit}}^{(n)}$ denotes the *critical cut-off* where the n^{th} Efimov-like trimer state emerges above the threshold in each case. In our EFT approach, the $\Lambda + u_0$ breakup threshold energies $\mathcal{E}_{2(s)}^{\text{thr}}$ of the $\Lambda\Lambda T$ ground state ($n = 0$) Efimov trimers are in effect identified with the ΛT spin-singlet dimer binding energies $\mathcal{B}_\Lambda[0^+]$, *vis-a-vis* the binding energies of the mirror Λ -hypernuclei (${}^4_\Lambda\text{H}$, ${}^4_\Lambda\text{He}$). The central values of these experimentally determined binding energies [5] (cf. Table. III) were used to extract the corresponding binding momenta $\gamma_{\Lambda T}$ used as input to our integrals equation. It is notable that irrespective of our choice of the spin-singlet (type A) or spin-triplet (type-B) ΛT subsystem in the elastic channel, our numerical evaluations only yield trimer level states deeper than the larger of the two particle-dimer breakup thresholds, namely, the $\Lambda + u_0$ thresholds. In other words, we find eigensolutions provided $B_{\Lambda\Lambda} > \mathcal{B}_\Lambda[0^+]$, i.e., for $\Lambda_c > \Lambda_{\text{crit}}^{(n=0)}$. The

Hypernucleus [J^p]	$B_\Lambda[J^+]$ (MeV) [5]	$\gamma_{\Lambda T} \overset{\uparrow}{\rightsquigarrow} (2\mu_{\Lambda T} B_\Lambda[J^+])^{1/2}$ (MeV)
${}^4_\Lambda\text{H} [0^+]$	2.04	$\gamma_0 \overset{\uparrow}{\rightsquigarrow} 57.078$
${}^4_\Lambda\text{H} (1^+)$	0.96	$\gamma_1 \overset{\uparrow}{\rightsquigarrow} 39.155$
${}^4_\Lambda\text{He} [0^+]$	2.39	$\gamma_0 \overset{\uparrow}{\rightsquigarrow} 61.779$
${}^4_\Lambda\text{He} (1^+)$	1.24	$\gamma_1 \overset{\uparrow}{\rightsquigarrow} 44.499$

TABLE III. Data for the binding energies $B_\Lambda[J^+]$ of the hypernuclear mirror states (${}^4_\Lambda\text{H}$, ${}^4_\Lambda\text{He}$) corresponding to the central values of the experimental results of Ref. [5]. In our EFT they are identified (symbol $\overset{\uparrow}{\rightsquigarrow}$) with the particle-dimer breakup threshold energies $-\mathcal{E}_{2(s)}^{thr}$ of the ground state ($n=0$) $\Lambda\Lambda T$ Efimov trimers, or equivalently, the $(\Lambda T)_s$ spin-singlet dimer binding energies [cf. Eq. (31)]. The binding momenta $\gamma_{\Lambda T}$ used as input to our integral equations are extracted from these data.

critical cut-offs for the ground states are tabulated earlier in Table. II. The eigenenergies are moreover sensitive to the input double- Λ scattering lengths which increase with increasing $|a_{\Lambda\Lambda}|$. Table. II also displays our cut-off values, $\Lambda_c = \Lambda_{\text{pot}}^{(n=0)}$ that reproduce the potential model double- Λ separation energies $B_{\Lambda\Lambda}$ of Ref. [8] as ground trimer state eigensolutions. Although $\Lambda_{\text{pot}}^{(n=0)}$ values are significantly larger than the usual hard scale of a pionless EFT, namely, $\Lambda_H \sim m_\pi$, they are in effect within a reasonable ballpark in context of hypernuclear systems where one-pion exchanges are forbidden by virtue of parity conservation. A more pertinent EFT hard scale consistent with the symmetries in this case may be taken as $\Lambda_H \sim 300 - 500$ MeV, with $\Lambda - \Lambda$ interactions predominantly known to be dominated by *two-pion-exchange* or the *σ -meson exchange* mechanism. However, it is conceivable that a momentum scale of this magnitude becomes inconsistent with the $\Lambda\Lambda T$ bound cluster ansatz, whereby the very existence of the core fields, $T \equiv t, h$ is questionable.

In figs. 5 and 6, with respect to the type-A and type-B elastic channels, we plot our predictions for the variations of the three-body binding energies $B_{\Lambda\Lambda}$, Eq.(28), with the inverse of the $\Lambda\Lambda$ -scattering lengths, i.e., $a_{\Lambda\Lambda}^{-1}$, using different values of the three-body couplings $g_3^{(A,B)}$ at appropriate cut-off scales Λ_c . Solutions to each set of integral equations [i.e., Eqns.(11) and (12)] is normalized to a single data point taken from Ref. [8], namely, ($B_{\Lambda\Lambda} = 2.96$ MeV, $a_{\Lambda\Lambda} = -0.5$ fm) for ${}^5_\Lambda\text{H}$ and ($B_{\Lambda\Lambda} = 3.605$ MeV, $a_{\Lambda\Lambda} = -0.5$ fm) for ${}^5_\Lambda\text{He}$. (cf. Table. II). In particular we find that for the choice of the cut-off scale, $\Lambda_c = 234$ MeV and correspondingly, $g_3^{(A)} = -6.4429$ and $g_3^{(B)} = -0.6669$ for ${}^5_\Lambda\text{H}$, and $g_3^{(A)} = -8.7568$ and $g_3^{(B)} = -0.7167$ for ${}^5_\Lambda\text{He}$, the double- Λ separation energies are predicted nearly the same as those from the cut-off independent potential model [8] (viz. for data points other than the normalizing point), as shown by the solid line curves in the figures. Consequently, in each case the

solid line curves are in effect our EFT determined calibration curves for determining $B_{\Lambda\Lambda}$ for any given value of the double- Λ scattering length.

The final part of our EFT analysis is concerned with the preliminary estimation of the S-wave three-body scattering lengths $a_{\Lambda\Lambda T}$, namely, the ${}^4_\Lambda\text{H} - \Lambda$ and ${}^4_\Lambda\text{He} - \Lambda$ scattering lengths. For this purpose, we numerically solve the two sets of coupled integral equations for the renormalized on-shell elastic K-matrix elements $\mathbb{K}_a^{A,B}(k, k)$ in each case [i.e., Eqs. (16) and (17)] which yield the scattering lengths in the threshold limit ($k \rightarrow 0$). Care must be taken to bypass the poles of the dimer propagators originating in the kinematical scattering domain close to the respective particle-dimer breakup thresholds. In this regard we have implemented a numerical methodology of solving a multi-dimensional generalization of principal value prescription modified integral equations, originally developed by Kowalski and Noyes [45, 46] (also see, Ref. [47]) for one-dimensional case.

Figures 7 and 8 display the cut-off scale dependence of the three-body scattering lengths, $a_{3(s)}$ and $a_{3(t)}$, respectively, for ${}^4_\Lambda\text{He}[0^+] - \Lambda$ and ${}^4_\Lambda\text{He}[1^+] - \Lambda$ scattering processes for several Nijmegen Soft-core potential model predicted double- Λ scattering lengths, namely, $a_{\Lambda\Lambda} = -0.50, -2.81, -10.6$ fm [33, 34]. The corresponding results the $\Lambda\Lambda t$ system being numerically close to the above results, we only display the $a_{3(s,t)}$ results for the $\Lambda\Lambda h$ system graphically, while a consolidated summary of our numerical predictions for both the $\Lambda\Lambda t$ and $\Lambda\Lambda h$ systems is tabulated in Table. IV. It is, however, worth mentioning that in contrast to our universal LO EFT approach with little observable difference between the $\Lambda\Lambda t$ and $\Lambda\Lambda h$ isospin partners, rather large isospin breaking corrections have been reported in these systems in existing potential model analyses, leading to significant differences in their predictions of two- and three-body binding energies [12, 48]. Such effects are perhaps captured in a subleading order EFT calculation which is beyond the scope of this analysis.

In the left panel plots of the above figures which exclude the three-body force in each case, the unregulated scattering amplitudes are evidently scale dependent and diverge for values of Λ_c associated with emerging three-body bound states. Such unphysical singularities in the scattering amplitude are renormalized by the introduction of the scale dependent contact couplings $g_3^{(A,B)}(\Lambda_c)$, as shown in the right panel plots which are free of singularities, smoothly decreasing with increasing Λ_c and ultimately converging onto the respective asymptotic values beyond $\Lambda_c \sim 400$ MeV. These asymptotic values are our EFT predicted three-body scattering lengths $a_{3(s,t)}$. Table. IV summarizes all our numerical values of the renormalized *spin-averaged* three-body scattering lengths ($a_{\Lambda\Lambda T}$) for the different input S-wave double- Λ scattering lengths ($a_{\Lambda\Lambda}$) taken from the recent phenomenological analyses using Dispersion Relations (DR) [18] and Relativistic Heavy-Ion Collisions (RHIC) [19], including also those due to the earlier mentioned $a_{\Lambda\Lambda}$ values of

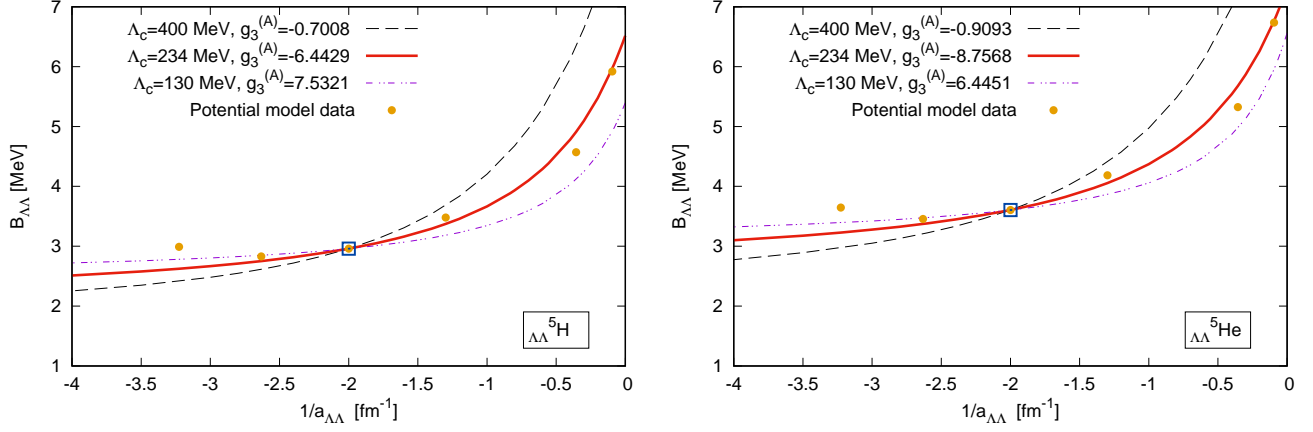


FIG. 5. The three-body binding (double- Λ separation) energy $B_{\Lambda\Lambda}$ of ${}^5_{\Lambda\Lambda}\text{H}$ (left panel) and ${}^5_{\Lambda\Lambda}\text{He}$ (right panel) versus the inverse of the S-wave double- Λ scattering length $a_{\Lambda\Lambda}^{-1}$ using different values of the three-body couplings $g_3^{(A)}$ at appropriate cut-off scales Λ_c . These results correspond to the type-A choice for the elastic channel using integral equations (11). The data points taken from the potential model analysis of Ref. [8] are displayed. In particular, the two data points, namely, $(B_{\Lambda\Lambda} = 2.96 \text{ MeV}, a_{\Lambda\Lambda} = -0.5 \text{ fm})$ for ${}^5_{\Lambda\Lambda}\text{H}$ and $(B_{\Lambda\Lambda} = 3.605 \text{ MeV}, a_{\Lambda\Lambda} = -0.5 \text{ fm})$ ${}^5_{\Lambda\Lambda}\text{He}$ (open squares) serve to normalize our results.

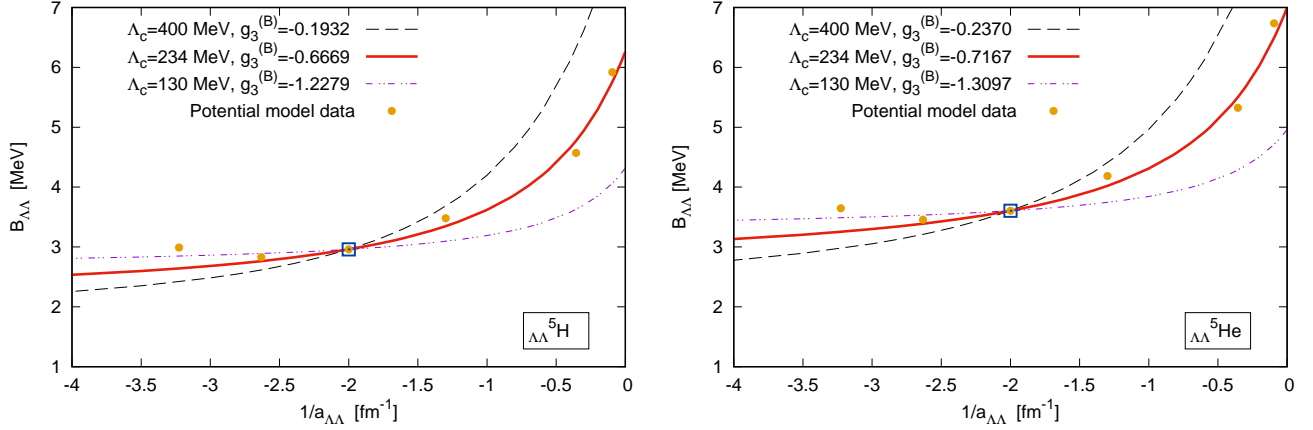


FIG. 6. The three-body binding (double- Λ separation) energy $B_{\Lambda\Lambda}$ of ${}^5_{\Lambda\Lambda}\text{H}$ (left panel) and ${}^5_{\Lambda\Lambda}\text{He}$ (right panel) versus the inverse of the S-wave double- Λ scattering length $a_{\Lambda\Lambda}^{-1}$ using different values of the three-body couplings $g_3^{(B)}$ at appropriate cut-off scales Λ_c . These results correspond to the type-B choice for the elastic channel using integral equations (12). The data points taken from the potential model analysis of Ref. [8] are displayed. In particular, the two data points, namely, $(B_{\Lambda\Lambda} = 2.96 \text{ MeV}, a_{\Lambda\Lambda} = -0.5 \text{ fm})$ for ${}^5_{\Lambda\Lambda}\text{H}$ and $(B_{\Lambda\Lambda} = 3.605 \text{ MeV}, a_{\Lambda\Lambda} = -0.5 \text{ fm})$ ${}^5_{\Lambda\Lambda}\text{He}$ (open squares) serve to normalize our results.

the Nijmegen Soft-core potential models (names within parentheses) [33, 34]. Notwithstanding the very wide range of $a_{\Lambda\Lambda}$ value taken as input, the variation in $a_{\Lambda\Lambda T}$ is rather nominal, although, individually the respective type-A and type-B renormalized scattering lengths, $a_{3(s)}$ and $a_{3(t)}$, do exhibit some degree of dependence on the input $(a_{\Lambda\Lambda}, B_{\Lambda\Lambda})$ values with $a_{3(s)}$ displaying a significantly more stronger dependence. However, the interesting observation is that the $(a_{\Lambda\Lambda}, B_{\Lambda\Lambda})$ dependence of $a_{3(s)}$ and $a_{3(t)}$ are quite the opposite, with $a_{3(s)}$ increasing and $a_{3(t)}$ decreasing with increasing $|a_{\Lambda\Lambda}|$ and decreasing $B_{\Lambda\Lambda}$. This feature of our results is depicted in the Phillips-line plots shown in fig. 9, with the ef-

fect that the resulting variation of the spin-averaged values of $a_{\Lambda\Lambda T}$ in the “physical” Phillips plot (shown in the lower panel) turns out to be quite moderate. The Phillips-line obtained for the type-A choice of the elastic channel (upper left panel) is in accordance with the usual expectation that the three-body binding energy is inversely related to the variation of the three-body scattering length which results in the characteristic negative slope of the Phillips plot. In contrast, the positive slope of the type-B Phillips plot (upper right panel) may seem quite counter-intuitive. Moreover the contrasting nature of the two results depending on the choice of the elastic channels is independent of the nature of the three-body

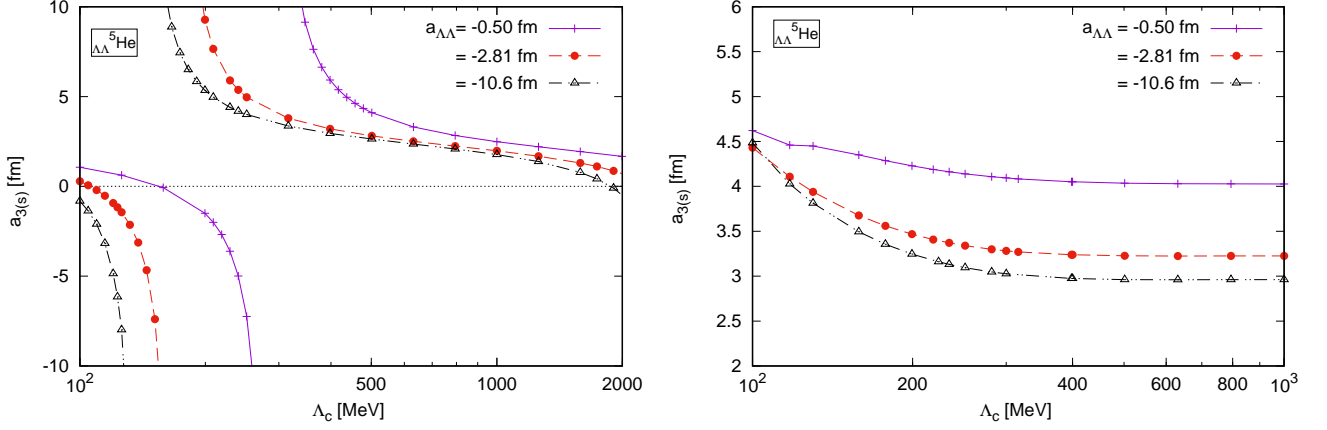


FIG. 7. The $J = 1/2$ S-wave three-body scattering length $a_{3(s)}$ for $\Lambda\Lambda h$ or ${}^4_\Lambda\text{He}[0^+] - \Lambda$ scattering versus the cut-off scale Λ_c without (left panel) and with (right panel) the three-body coupling $g_3^{(A)}$, for different values of the Nijmegen Soft-core potential model double- Λ scattering lengths, namely, $a_{\Lambda\Lambda} = -0.5, -2.81$, and -10.6 fm, obtained from Refs. [33, 34]. The input double- Λ binding energies $B_{\Lambda\Lambda}$ needed to fix $g_3^{(A)}(\Lambda_c)$ in the right panel plot corresponding to $a_{\Lambda\Lambda} = -2.81$, and -10.6 fm are obtained using the calibration (solid line) curves of fig. 5 (also see Table. IV), while for $a_{\Lambda\Lambda} = -0.5$ fm $B_{\Lambda\Lambda}$ is taken from Ref. [8] and used as the normalization point. The counterpart plots for the $\Lambda\Lambda t$ or ${}^4_\Lambda\text{H}[0^+] - \Lambda$ scattering having barely any discernible difference from the above plots are not displayed.

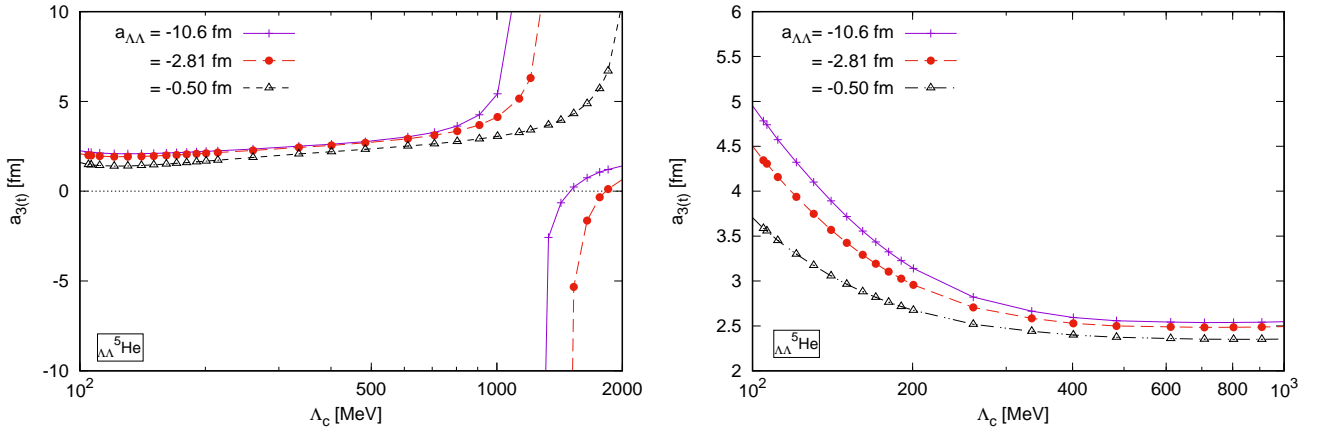


FIG. 8. The $J = 1/2$ S-wave three-body scattering length $a_{3(t)}$ for $\Lambda\Lambda h$ or ${}^4_\Lambda\text{He}[1^+] - \Lambda$ scattering versus the cut-off scale Λ_c without (left panel) and with (right panel) the three-body coupling $g_3^{(B)}$, for different values of the Nijmegen Soft-core potential model double- Λ scattering lengths, namely, $a_{\Lambda\Lambda} = -0.5, -2.81$, and -10.6 fm, obtained from Refs. [33, 34]. The input double- Λ binding energies $B_{\Lambda\Lambda}$ needed to fix $g_3^{(B)}(\Lambda_c)$ in the right panel plot corresponding to $a_{\Lambda\Lambda} = -2.81$, and -10.6 fm are obtained using the calibration (solid line) curves of fig. 5 (also see Table. IV), while for $a_{\Lambda\Lambda} = -0.5$ fm $B_{\Lambda\Lambda}$ is taken from Ref. [8] and used as the normalization point. The counterpart plots for $\Lambda\Lambda t$ or ${}^4_\Lambda\text{H}[1^+] - \Lambda$ scattering having barely any discernible difference from the above plots are not displayed.

force and the renormalization schemes we have adopted (cf. footnote 1). This is revealed from the same contrasting behaviors apparent to the unrenormalized scattering length plots in the left panels of figs. 7 and 8. It is notable here that in determining $a_{3(s)}$, only the dynamics near the deeper threshold, namely, the particle-singlet-dimer threshold is relevant, while the dynamics of both thresholds contribute in determining $a_{3(t)}$. Although the root cause of this contrasting behavior is unclear, a plau-

sible reasoning may be inherent to the off-shell nature of the underlying dynamics arising from the complex interplay between the two particle-dimer thresholds.

To test this hypothesis we took the strategy of considering a hypothetical (unphysical) scenario in which the triplet and singlet ΛT subsystems were completely decoupled to avoid the simultaneous contribution of the two particle-dimer thresholds for each of the type-A and type-B $\Lambda\Lambda T$ systems. In other words this tantamount

Hypernucleus ($J = \frac{1}{2}$)	Scattering length $a_{\Lambda\Lambda}$ (fm)	Separation Energy $B_{\Lambda\Lambda}$ (MeV) [8]	Type-A $B_{\Lambda\Lambda}$ (MeV)	Type-A $a_{3(s)}$ (fm)	Type-B $B_{\Lambda\Lambda}$ (MeV)	Type-B $a_{3(t)}$ (fm)	($2J + 1$) average $a_{\Lambda\Lambda T}$ (fm)
${}^5_{\Lambda\Lambda}\text{H}$	-0.50 (NSC97e) [33, 34]	2.960	2.960	4.53	2.960	2.33	3.03
	-0.31 (ND) [33, 34]	2.990	2.624	5.30	2.642	2.28	3.30
	-0.38 (NSC97b) [33, 34]	2.830	2.752	4.94	2.763	2.30	3.17
	-0.60 (DR) [18]	-	3.122	4.31	3.112	2.35	2.96
	-0.77 (ND) [33, 34]	3.480	3.373	4.06	3.347	2.37	2.89
	-1.20 (DR) [18]	-	3.884	3.73	3.823	2.41	2.80
	-1.25 (RHIC) [19]	-	3.934	3.71	3.869	2.42	2.80
	-1.80 (DR) [18]	-	4.385	3.53	4.288	2.44	2.75
	-2.81 (ND) [33, 34]	4.570	4.911	3.37	4.774	2.45	2.70
-10.6 (ESC00) [33, 34]	5.920	5.973	3.16	5.757	2.46	2.65	
${}^5_{\Lambda\Lambda}\text{He}$	-0.50 (NSC97e) [33, 34]	3.605	3.605	4.03	3.605	2.35	2.86
	-0.31 (NSC97e) [33, 34]	3.645	3.228	4.54	3.254	2.30	3.02
	-0.38 (NSC97b) [33, 34]	3.455	3.373	4.30	3.389	2.32	2.94
	-0.60 (DR) [18]	-	3.783	3.87	3.770	2.37	2.82
	-0.77 (ND) [33, 34]	4.185	4.055	3.69	4.021	2.41	2.78
	-1.20 (DR) [18]	-	4.603	3.43	4.523	2.45	2.73
	-1.25 (RHIC) [19]	-	4.656	3.41	4.571	2.46	2.73
	-1.80 (DR) [18]	-	5.130	3.26	5.004	2.48	2.70
	-2.81 (ND) [33, 34]	5.325	5.677	3.14	5.503	2.51	2.68
-10.6 (ESC00) [33, 34]	6.735	6.766	2.96	6.494	2.53	2.64	

TABLE IV. Our predictions for the $J = 1/2$ S-wave three-body scattering lengths $a_{\Lambda\Lambda T}$ [cf. Eq. (24)] of the double- Λ mirror hypernuclei (${}^5_{\Lambda\Lambda}\text{H}$, ${}^5_{\Lambda\Lambda}\text{He}$) obtained for several S-wave scattering length $a_{\Lambda\Lambda}$ taken from various phenomenological analyses, e.g., Nijmegen Soft-core potential model (names within parentheses) [33, 34], Dispersion Relations (DR) [18] and Relativistic Heavy-Ion Collisions (RHIC) [19]. All the input values of the double- Λ separation energies $B_{\Lambda\Lambda}$, with the exception of the respective normalizing points (i.e., for $a_{\Lambda\Lambda} = -0.50$ fm with $B_{\Lambda\Lambda}$ values directly taken from Ref. [8]), are obtained as predictions from our EFT calibration (solid line) curves in figs. 5 and 6. For comparison the values of $B_{\Lambda\Lambda}$ calculated from the incremental binding energies $\Delta B_{\Lambda\Lambda}$ [cf. our Eq. (28)] of Table. VIII of Ref. [8] are also displayed.

to removing the contributions of the triplet dimer field u_1 in the type-A integral equations (11), and the singlet dimer field u_0 in the type-B integral equations (12). The resulting new $\Lambda\Lambda T$ systems become considerably simpler reducing each set into a system of two coupled channel integral equations. It was found that the reduced systems with the type-A elastic channels did not exhibit a limit cycle behavior any longer while the ones with the type-B elastic channels continued to exhibit the limit cycles but instead following a very different value of the asymptotic parameter, namely, $s'_0{}^\infty \approx 0.84 \dots$ for each mirror hypernucleus. Nevertheless, an estimation of the respective scattering lengths $a_{3(s)}$ and $a_{3(t)}$ in that case indeed led to the expected negative slope Phillips-lines. Such a scenario ostensibly suggests possible role of the simultaneous particle-dimer threshold dynamics resulting in the atypical nature of the type-B Phillips-line. A more satisfactory explanation of this feature perhaps requires an thorough understanding of the off-shell dynamics demanding a four-body calculations that is beyond our present scope. At the same time, the fact that our results converge asymptotically for momentum scales significantly larger than the m_π , the canonical hard scale of $\not\epsilon$ EFT, clearly indicate a considerable degree of insensitivity of $\Lambda\Lambda T$ three-body dynamics to the $\Lambda-\Lambda$ correlations. In this regard our findings corroborate the two previous $\not\epsilon$ EFT works [27, 28] on similar three-body calculations of ${}^4_{\Lambda\Lambda}\text{H}$ and ${}^6_{\Lambda\Lambda}\text{He}$ double- Λ hypernuclei.

IV. SUMMARY AND CONCLUSIONS

In summary, the work presents an assay of the putative doubly strange ($S = -2$) mirror $\Lambda\Lambda$ -hypernuclei (${}^5_{\Lambda\Lambda}\text{H}$, ${}^5_{\Lambda\Lambda}\text{He}$) in the context of a LO pionless EFT. In this framework such systems are conjectured as shallow three-particle bound halo clusters, viz. the iso-doublet partners ($\Lambda\Lambda t$, $\Lambda\Lambda h$) in the $J = 1/2$ channel. The numerical methodology presented here closely followed the approaches of Refs. [27–30]. In this framework one needs to solve the Faddeev-like coupled integral equations [40–43] to study the dynamical interplay between the different constituent two-body subsystems, namely, the virtual bound ${}^1\text{S}_0$ $\Lambda\Lambda$ cluster (with $a_{\Lambda\Lambda} < 0$), and the Λt or Λh ${}^1\text{S}_0$ and ${}^3\text{S}_1$ bound clusters (equivalently, the two-body spin-singlet and -triplet bound states, i.e., ${}^4_{\Lambda}\text{H}[J = 0^+, 1^+]$ and ${}^4_{\Lambda}\text{He}[J = 0^+, 1^+]$), which can plausibly emerge into three-body universal bound states. This is evidenced in our analysis by the fact that the RG running of the three-body couplings $g_3^{(A,B)}(\Lambda_c)$ for these three-body systems follow limit cycles. This implies that in the *unitary limit* a discrete sequence of Efomov states emerges from zero energy threshold [31], and simultaneously with our LO theory in the *scaling limit* the ground state energy collapses to negative infinity (Thomas effect [49]). However, such universal effects are *de facto* unrealistic and disappear for finite range (momentum

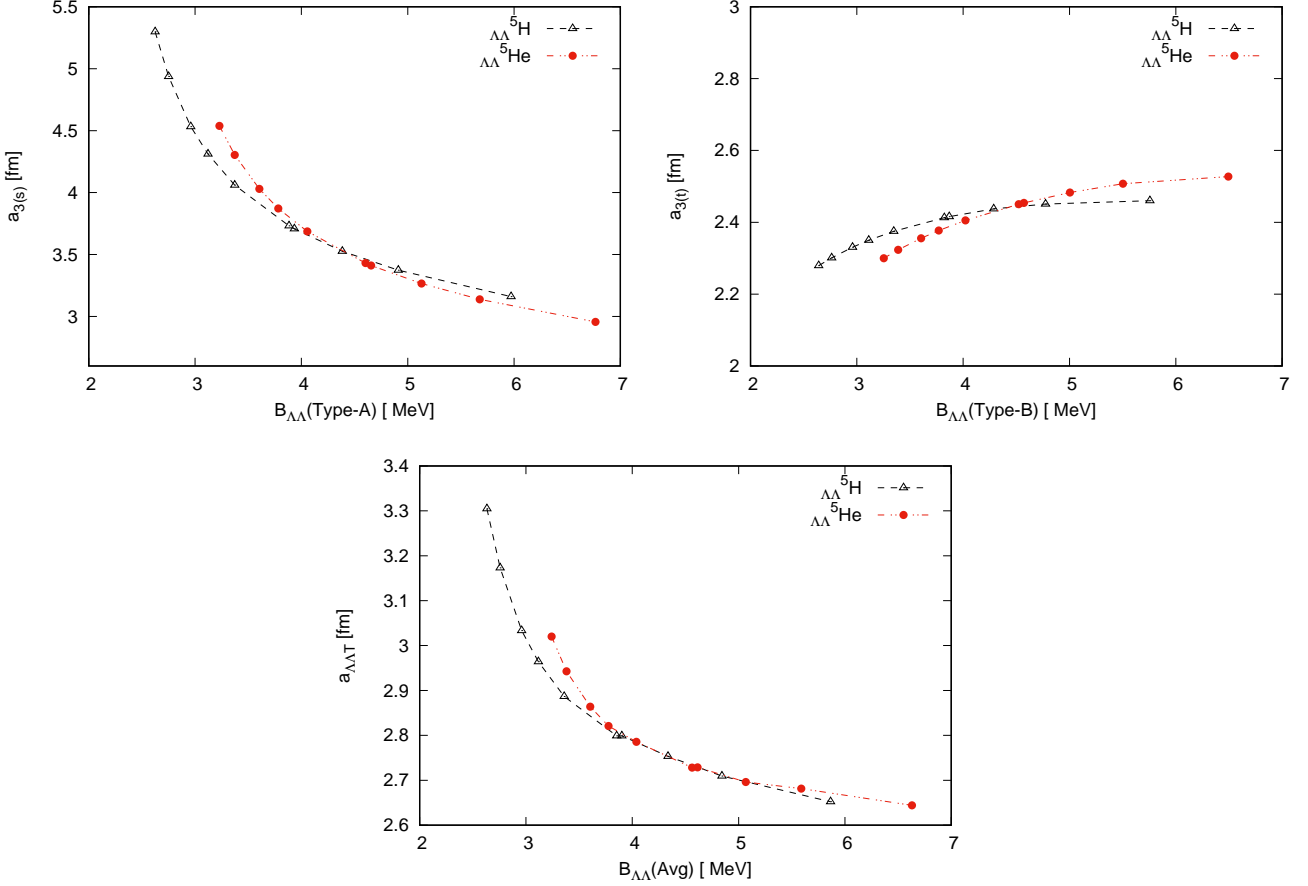


FIG. 9. Phillips-line plot for the type-A elastic channel, i.e., ${}^4_{\Lambda}\text{He}[0^+] - \Lambda$ scattering (upper left panel) and the type-B elastic channel, i.e., ${}^4_{\Lambda}\text{He}[1^+] - \Lambda$ scattering (upper right panel) are displayed. The lower panel displays the “physical” Phillips-line corresponding to the spin-average scattering length $a_{\Lambda\Lambda T}$ plotted against the mean of the type-A and type-B values of the three-body binding energies obtained from Table. IV, namely, $B_{\Lambda\Lambda}(\text{Avg}) = \frac{1}{2}[B_{\Lambda\Lambda}(\text{Type-A}) + B_{\Lambda\Lambda}(\text{Type-B})]$.

cut-off) interaction and small scattering lengths. Nevertheless, for the low-energy $\Lambda\Lambda t$ or $\Lambda\Lambda h$ clusters, sufficiently far from other open channels and with reasonably fine-tuned $\Lambda\Lambda$ correlation strengths, as parametrized by the double- Λ scattering lengths predicted from several phenomenological models [18, 19, 33, 34], it is conceivable that any remnant universal effects may lead to the formation of the Efimov-like bound mirror hypernuclei, ${}^5_{\Lambda\Lambda}\text{H}$ and ${}^5_{\Lambda\Lambda}\text{He}$.

Our analysis shows that with the finite choice of the two-body scattering lengths and appropriate strengths of the three-body couplings close to cut-off scales $\Lambda_c \sim 230 - 240$ MeV (fixed using the RG limit cycles), we obtain fairly good agreements with existing potential model data on the separation energies $B_{\Lambda\Lambda}$ for each $\Lambda\Lambda$ -hypernuclei from a prominent Faadeev calculation analysis [8]. This agreement, however, relies on the normalization of our solution sets with respect to a single potential model data point (shown as squares for each mirror hypernuclei in figs. 5 and 6.) Here $B_{\Lambda\Lambda}$ can be identified with the eigenenergy of the ground state

($n = 0$) Efimov trimer provided that the $\not\#$ EFT analysis can be extended to include σ -meson or two-pion-exchange interactions in hyperonic systems with adjusted hard scale, $\Lambda_H \sim 300 - 500$ MeV. But whether such states in this framework can be supported as physically realizable bound states is debatable depending crucially on support from experimental or lattice QCD simulations data which are currently altogether missing. Feasibility studies from the much awaited production experiments, like the PANDA and CBM at FAIR [50–52], and JPARC-P75 [53], may in future be able to explicate the inherent character of these systems. Besides, predictions based on LO analyses are by and large qualitative in nature and must be supplemented by subleading order EFT analyses for a robust assessment of the feasibility of such states. This should naturally address issues like the compatibility of the low-energy $\Lambda\Lambda T$ cluster picture at momentum scales $\gtrsim \Lambda_H$ that potentially probe the short-range degrees of freedom beyond the breakup of the helion (h) or triton (t) core fields.

Finally, as a demonstration of the predictive power of

our EFT analysis, we presented preliminary estimates of the *a priori* undetermined three-body scattering lengths $a_{\Lambda\Lambda T}$ for the S-wave ${}^4_{\Lambda}\text{H} - \Lambda$ and ${}^4_{\Lambda}\text{He} - \Lambda$ scattering processes. The results crucially depend on the precise nature of the $B_{\Lambda\Lambda}$ versus $a_{\Lambda\Lambda}$ correlations. Subject to the limitations of EFT's predictive power up to setting of a single normalizing data point and subsequent fixing of three-body couplings $g_3^{(A,B)}$ to ensure good match with the pre-existing potential model data, the $(B_{\Lambda\Lambda}, a_{\Lambda\Lambda})$ calibration plots were self-consistently used to predict $a_{3(s)}$ and $a_{3(t)}$. The fact that the asymptotic values of the renormalized $a_{3(s,t)}$ were obtained for $\Lambda_c \gtrsim 400 - 500$ MeV, which is well beyond the hard scale of ${}^{\#}\text{EFT}$, suggests that the three-body dynamics are likely to become insensitive to the low-energy $\Lambda - \Lambda$ interactions in the cluster EFT picture, unless the hard scale Λ_H can be extended sufficiently beyond. This supports the conclusions made in Refs. [27, 28] also based on similar three-body analyses of double- Λ hypernuclear cluster, such as ${}_{\Lambda\Lambda}{}^4\text{H}$ and ${}_{\Lambda\Lambda}{}^6\text{He}$. High-momentum mechanisms beyond the realm of the current EFT framework can play a significant role in the formation of such bound states. Of course, this also does not preclude plausible underlying low-energy off-shell mechanisms leading to effects, such as the unusual nature of the Phillips-lines associated with the type-B three-body scattering lengths $a_{3(t)}$ (cf. upper right panel in figs. 9), that is not perhaps straightforwardly explicated without partaking an involved four-body calculation. Such an endeavour goes well beyond the scope of the current qualitative analysis of this work.

ACKNOWLEDGMENTS

We are thankful to Shung-Ichi Ando for providing many useful suggestions to this work.

V. APPENDIX

A. One- and Two-body non-relativistic Propagators

Here we summarize the one- and two-body non-relativistic propagators specific to the $\Lambda\Lambda T$ three-body systems in pionless effective theory (${}^{\#}\text{EFT}$). In this framework, at sufficiently low-energies below the respective

break-up scales, we may consider the triton (${}^3\text{H}$ or t) and the helion (${}^3\text{He}$ or h) as being fundamental particles. Thus, as the fundamental one-body components of the theory, the Λ and T propagators are, respectively, given as

$$\begin{aligned} iS_{\Lambda}(p_0, \mathbf{p}) &= \frac{i}{p_0 - \frac{p^2}{2M_{\Lambda}} - i\eta}, \\ iS_T(p_0, \mathbf{p}) &= \frac{1}{p_0 - \frac{p^2}{2M_T} - i\eta}, \end{aligned} \quad (32)$$

where p_0 and \mathbf{p} are the generic off-shell energy and three-momentum. In our analysis we only consider the S-waves contributions from the two-body interactions at LO. We have incorporated a power counting scheme [20, 21] for the ${}^1\text{S}_0$ $\Lambda - T$, ${}^3\text{S}_1$ $\Lambda - T$ and the ${}^1\text{S}_0$ $\Lambda - \Lambda$ interactions in the two-body sector, in which the unitarized two-body amplitudes are conveniently expressed in terms of the auxiliary dimer fields, namely, the spin-singlet and spin-triplet ΛT fields $u_{0,1}$, and the spin-singlet $\Lambda\Lambda$ u_s field. The leading order renormalized and dressed dimer propagators [24, 27–29, 37] are given by (see fig. 10)

$$\begin{aligned} i\Delta_0(p_0, \mathbf{p}) &= \frac{2\pi}{y_0^2 \mu_{\Lambda T}} \frac{i}{\gamma_0 - \sqrt{-2\mu_{\Lambda T}(p_0 - \frac{\mathbf{p}^2}{2(M_T + M_{\Lambda})})} - i\eta}, \\ i\Delta_1(p_0, \mathbf{p}) &= \frac{2\pi}{y_1^2 \mu_{\Lambda T}} \frac{i}{\gamma_1 - \sqrt{-2\mu_{\Lambda T}(p_0 - \frac{\mathbf{p}^2}{2(M_T + M_{\Lambda})})} - i\eta}, \\ i\Delta_s(p_0, \mathbf{p}) &= \frac{4\pi}{y_s^2 M_{\Lambda}} \frac{i}{\frac{1}{a_{\Lambda\Lambda}} - \sqrt{-M_{\Lambda}(p_0 - \frac{\mathbf{p}^2}{4M_{\Lambda}})} - i\eta}, \end{aligned} \quad (33)$$

where, γ_0 and γ_1 , respectively, are the binding momenta of spin-singlet and spin-triplet states of ΛT , and $a_{\Lambda\Lambda}$ is S-wave double- Λ scattering length.

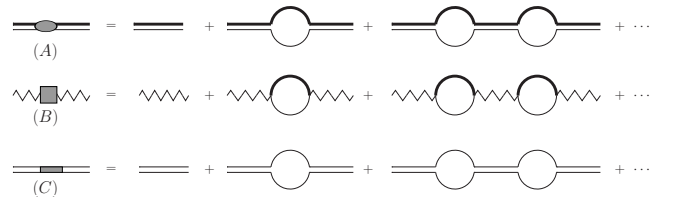


FIG. 10. Diagrams for the renormalized dressed dimer propagators: (A) $i\Delta_0$ for the spin-singlet auxiliary field u_0 , (B) $i\Delta_1$ for the spin-triplet auxiliary field u_1 , and (C) $i\Delta_s$ for the spin-singlet auxiliary field u_s . Thick (thin) lines denote the Λ -hyperon (core $T \equiv t, h$) field propagators.

[1] H. Takahashi *et al.*, Phys. Rev. Lett. **87**, 212502 (2001).
[2] J. K. Ahn *et al.*, Phys. Rev. Lett. **87**, 132504 (2001).
[3] D. H. Davis, Nucl. Phys. A **754** (2005) 3c.
[4] J. K. Ahn *et al.* [E373 (KEK-PS) Collaboration], Phys. Rev. C **88**, no. 1, 014003 (2013).

[5] H. Tamura *et al.*, Nucl. Phys. A **914**, 99 (2013).
[6] R. L. Jaffe, Phys. Rev. Lett. **38**, 195 (1977)
[7] H. W. Hammer, Nucl. Phys. A **705**, 173 (2002)
[8] I. N. Filikhin and A. Gal, Nucl. Phys. A **707**, 491 (2002).

- [9] I. N. Filikhin, A. Gal and V. M. Suslov, Phys. Rev. C **68**, 024002 (2003).
- [10] H. Nemura, Y. Akaishi and K. S. Myint, Phys. Rev. C **67**, 051001 (2003)
- [11] K. S. Myint, S. Shinmura and Y. Akaishi, Eur. Phys. J. A **16**, 21 (2003)
- [12] D. E. Lansky and Y. Yamamoto, Phys. Rev. C **69**, 014303 (2004)
- [13] M. Shoeb, Phys. Rev. C **69**, 054003 (2004).
- [14] H. Nemura, S. Shinmura, Y. Akaishi and K. S. Myint, Phys. Rev. Lett. **94**, 202502 (2005).
- [15] H. Nemura, S. Shinmura, Y. Akaishi and K. S. Myint, Nucl. Phys. A **754**, 110 (2005).
- [16] S. R. Beane *et al.* [NPLQCD Collaboration], Phys. Rev. Lett. **106**, 162001 (2011).
- [17] T. Inoue, *et al.* [HAL QCD Collaboration], Phys. Rev. Lett. **106**, 162002 (2011).
- [18] A. M. Gasparyan, J. Haidenbauer and C. Hanhart, Phys. Rev. C **85**, 015204 (2012)
- [19] K. Morita, T. Furumoto and A. Ohnishi, Phys. Rev. C **91**, no. 2, 024916 (2015)
- [20] D. B. Kaplan, M. J. Savage and M. B. Wise, Phys. Lett. B **424**, 390 (1998).
- [21] D. B. Kaplan, M. J. Savage and M. B. Wise, Nucl. Phys. B **534**, 329 (1998).
- [22] U. van Kolck, Nucl. Phys. A **645**, 273-302 (1999).
- [23] P. F. Bedaque, H. W. Hammer and U. van Kolck, Phys. Rev. Lett. **82**, 463 (1999).
- [24] P. F. Bedaque, H. W. Hammer and U. van Kolck, Nucl. Phys. A **646**, 444 (1999).
- [25] P. F. Bedaque, H. W. Hammer and U. van Kolck, Nucl. Phys. A **676**, 357 (2000).
- [26] E. Braaten and H.-W. Hammer, Phys. Rept. **428**, 259 (2006).
- [27] S.-I. Ando, G.-S. Yang and Y. Oh, Phys. Rev. C **89**, 014318 (2014).
- [28] S.-I. Ando and Y. Oh, Phys. Rev. C **90**, 037301 (2014).
- [29] S. I. Ando, U. Raha and Y. Oh, Phys. Rev. C **92**, no. 2, 024325 (2015).
- [30] U. Raha, Y. Kamiya, S. I. Ando, and T. Hyodo, Phys. Rev. C **98**, no. 3, 034002 (2018).
- [31] V. Efimov, Phys. Lett. B **33**, 563 (1970).
- [32] F. Hildenbrand and H.-W. Hammer, Phys. Rev. C **100**, 034002 (2019).
- [33] R. H. Dalitz *et al.*, Proc. Roy. Soc. London A **426**, 1-17 (1989).
- [34] V. G. J. Stoks and Th. A. Rijken, Phys. Rev. C **59**, 3009 (1999).
- [35] S. R. Beane and M. J. Savage, Nucl. Phys. A **694**, 511 (2001).
- [36] S.-I. Ando and C. H. Hyun, Phys. Rev. C **72**, 014008 (2005).
- [37] S. I. Ando and M. C. Birse, J. Phys. G **37**, 105108 (2010).
- [38] H. W. Griesshammer, Nucl. Phys. A **744**, 192 (2004).
- [39] K. G. Wilson, Phys. Rev. D **3**, 1818 (1971).
- [40] G. V. Skornyakov and K. A. Ter-Martirosyan, Sov. Phys. JETP **4**, 648 (1957) [Zh. Eksp. Teor. Fiz. **31**, 775 (1956)].
- [41] G. V. Skornyakov and K. A. Ter-Martirosyan, JETP **31**, 775 (1956).
- [42] G. S. Danilov, Zh. Eksp. Teor. **40**, 498 (1961) [Sov. Phys. JETP **13**, 349 (1961)].
- [43] G. S. Danilov and V. I. Lebedev, Sov. Phys. JETP **17**, 1015 (1963).
- [44] P. J. Mohr, D. B. Newell and B. N. Taylor, Rev. Mod. Phys. **88**, no.3, 035009 (2016).
- [45] K. L. Kowalski, Phys. Rev. Lett. **15**, 798 (1965).
- [46] H. P. Noyes, Phys. Rev. Lett. **15**, 538 (1965).
- [47] W. Glöckle, *The Quantum Mechanical Few-Body Problem*, (Text and Monographs in Physics, Springer-Verlag, Heidelberg, 1983).
- [48] A. Gal, Phys. Lett. B **744**, 352 (2015).
- [49] L. H. Thomas, Phys. Rev. **47**, 903 (1935).
- [50] J. Pochodzalla *et al.* [PANDA Collaboration], EPJ Web of Conferences **3**, 07008 (2010).
- [51] G. Boca *et al.* [PANDA Collaboration], EPJ Web of Conferences **95**, 01001 (2015).
- [52] G. Vassiliev *et al.* [CBM Collaboration], JPS Conf. Proc., **092001** (2017).
- [53] H. Fujioka *et al.* [JPARC Collaboration], AIP Conference Proceedings **2130**, 040002 (2019).